Insights from geodynamical modeling on possible fates of continental mantle lithosphere: Collision, removal, and overturn

Article *in* Canadian Journal of Earth Sciences · April 2010

DOI: 10.1139/E09-043

CITATIONS
31

READS
156

5 authors, including:

Russell Pysklywec
University of Toronto
90 PUBLICATIONS **1,854** CITATIONS
SEE PROFILE

Oguz H. Göğüş
Istanbul Technical University
70 PUBLICATIONS **725** CITATIONS
SEE PROFILE

John A. Percival
Natural Resources Canada
162 PUBLICATIONS **4,350** CITATIONS
SEE PROFILE

A. R. Cruden
Monash University (Australia)
177 PUBLICATIONS **4,719** CITATIONS
SEE PROFILE

Insights from geodynamical modeling on possible fates of continental mantle lithosphere: collision, removal, and overturn[1]

Russell N. Pysklywec, Oguz Gogus, J. Percival, A.R. Cruden, and C. Beaumont

Abstract: Geodynamic modeling demonstrates various modes of behaviour of the tectonically active continental mantle lithosphere. At continental collision, mantle lithosphere below thickening crust can be accommodated by mixed subduction-like consumption and viscous drip-like instability, depending on the material rheology, temperature, and convergence velocity. Late-stage slab steepening, dual-sided and ablative consumption, and breakoff can occur as the buoyant crust resists subduction. Removal of accreted crust by erosion can modify how even the deepest portions of the mantle lithosphere evolves during contraction. When gravitational forcing rather than plate shortening dominates, mantle lithosphere may be removed through viscous dripping-like instability or delamination. The removal induces crustal heating, modified topography, and deformation, but distinctive styles of these develop depending on whether mantle lithosphere delaminates or drips. With a modified density stratification postulated for the Archean, relatively buoyant mantle lithosphere may undergo an in-situ overturn when triggered by unstable dense eclogite and basal traction. This causes a pulse of rapid crustal heating as hot lowermost lithosphere is brought into contact with the base of the crust. As an interpretive tool, the geodynamic experiments illustrate some of the dynamically feasible modes of behaviour and controlling parameters for the continental mantle lithosphere in ancient to modern tectonic environments.

Résumé : La modélisation géodynamique offre divers modèles de comportement du manteau lithosphérique continental tectoniquement actif. Lors de la collision continentale, le manteau lithosphérique sous la croûte qui s'épaissit peut s'adapter par une consommation combinée de type subduction et d'instabilité de type égouttement visqueux, selon la rhéologie du matériel, la température et la vitesse de convergence. Une accentuation de phase tardive de la pente de la dalle, une consommation ablative – à deux côtés et le décrochement de la dalle peuvent avoir lieu alors que la croûte flottante résiste à la subduction. Le retrait par érosion de la croûte accrétée peut modifier même la manière dont les portions les plus profondes du manteau lithosphérique évoluent durant la contraction. Lorsque le forçage gravitationnel domine plutôt que le raccourcissement des plaques, il peut y avoir retrait du manteau lithosphérique par une instabilité de type égouttement visqueux ou par délamination. Le retrait cause l'échauffement de la croûte, la modification de la topographie et de la déformation mais les styles distincts de ces effets dépendent de la délamination ou de l'égouttement de la lithosphère. En postulant une stratification à densité modifiée pour l'Archéen, la lithosphère du manteau, relativement légère et flottante, peut subir un renversement in situ s'il est déclenché par une éclogite dense et instable et de la traction à la base. Cela cause un échauffement rapide de la croûte alors que la chaude lithosphère inférieure est amenée en contact avec la base de la croûte. Servant d'outils d'interprétation, les essais géodynamiques illustrent quelques-uns des modes de comportement dynamiquement réalisables et des paramètres de contrôle de la lithosphère du manteau continental dans des environnements tectoniques anciens à modernes.

[Traduit par la Rédaction]

Received 19 August 2009. Accepted 21 August 2009. Published on the NRC Research Press Web site at cjes.nrc.ca on 4 May 2010.

Paper handled by Associate Editor R. Clowes.

R.N. Pysklywec,[2] O. Gogus, and A.R. Cruden. Department of Geology, University of Toronto, Toronto, ON M5S 3B1, Canada.
J. Percival. Geological Survey of Canada, 601 Booth St, Ottawa, ON K1A 0E8, Canada.
C. Beaumont. Department of Oceanography, Dalhousie University, Halifax, NS B3H 4J1, Canada.

[1]This article is one of a series of papers published in this Special Issue on the theme *Lithoprobe — parameters, processes, and the evolution of a continent*.

[2]Corresponding author (e-mail: russ@geology.utoronto.ca).

Introduction

The sub-crustal portion of the lithosphere, the mantle lithosphere, comprises the bulk of the continental lithosphere. Compared to the crust, the structure, composition, and dynamics of the continental mantle lithosphere are rather poorly understood. This is due to several factors: the inherent difficulty of studying a remote region through the thick (potenially highly deformed) continental crust, the possibly heterogeneous nature of the continental lithosphere, and the relative inactivity of this part of the lithosphere. As an example, even at the active continental collision zones on Earth where continental mantle lithosphere is clearly tectonically active and deforming, the mechanism by which the convergence of mantle lithosphere is accommodated is uncertain. In comparison, the subduction behaviour of ocean

lithosphere at plate convergence is well constrained. The morphology of the descending ocean crust and mantle lithosphere in the upper mantle is "illuminated" by seismic energy as the Wadati-Benioff zone. Furthermore, the thinner oceanic lithosphere is much less heterogeneous than continental lithosphere and, in some cases, large-scale sections of mantle lithosphere are exposed at the surface in obducted terranes.

Aspects of the mantle lithosphere may be deduced through direct observation of surface geology and indirect methods of geophysical imaging at depth. Such studies have been a substantial and significant part of project Lithoprobe. Seismic anisotropy and receiver function studies, for example, show mantle lithospheric "stratigraphy" that may indicate construction of the Slave craton by shallow subduction-like processes (Bostock 1997, 1998). For the same region, deep magnetotelluric surveys reveal the presence of conductivity anomalies in the sub-crustal lithosphere that may reflect chemical alterations associated with terrane accretion events (Jones et al. 2001). Reflection features from seismic imaging have been correlated between the crust and mantle, and interpreted as the possible remnant structure of Archean subduction within the Superior Province (Calvert et al. 1995). Abundant geochemical data from mantle xenoliths and volcanic extrusions have allowed for inferences to be made about the composition and genesis of the continental mantle lithosphere for various Archean and Proterozoic terranes (e.g., Schmidberger and Francis 1999; Kopylova and Russell 2000; Carbno and Canil 2002; Scully et al. 2004). It is not the goal here to review such studies comprehensively; rather, readers are referred to Theme 2 of this Special Issue for an overview of Lithoprobe work on the sub-crustal lithosphere.

The main focus of our Lithoprobe related research has been to study the dynamics of the continental mantle lithosphere and the relationship between these dynamics and the evolution of the crust. As such, the work bridges the crust and mantle; traditionally separate areas of study in geodynamics research. For the research, we use numerical and physical scaled analogue techniques to make idealized models of the upper mantle and crust. Forward modeling permits the investigation of complex non-linear physical systems, like the deforming and heterogeneous surface and near-surface layers of the Earth. Modeling experiments can be devised to evaluate modes of behaviour that are dynamically feasible and consider how these behaviours may relate to (more visible) crustal tectonics. The thermomechanical configuration of such experiments can be readily modified to treat diverse tectonic environments ranging between present-day to inferred Archean conditions. In addition, numerical experiments can be run relatively easily, allowing for analyses of wide ranges of often poorly constrained physical parameters.

Here, we present geodynamic experiments that investigate three fundamental behavioural styles of the continental mantle lithosphere. Specifically, we explore

(1) the process by which mantle lithosphere is accommodated during plate convergence and continental collision;
(2) mechanisms that account for removal of the mantle lithosphere and the surface expression of such events;
(3) in situ overturn of mantle lithosphere and its thermal consequences for the crust.

Fig. 1. Schematic of upper mantle-scale geodynamic models and outline of model sets. Expt., experiment; ρ, density; v, plate convergence velocity.

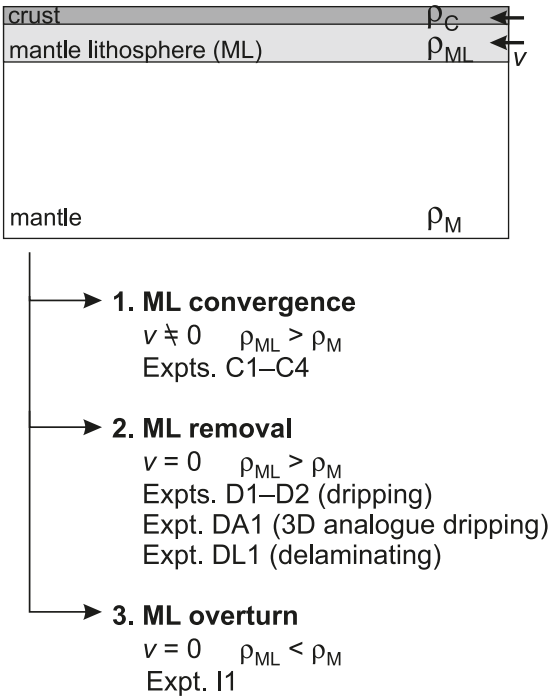

Figure 1 illustrates the different model sets relating to each of these. The models are upper-mantle scale with full dynamical coupling between the crust, mantle lithosphere, and mantle, with the exception of model I1, which treats the sub-lithospheric mantle as a basal boundary condition. At the scale we are considering, the primary driving forces in the models are gravitational and those associated with large-scale plate motion. Accordingly, the model sets listed in Fig. 1 are differentiated largely by variations in the material buoyancy (which gives rise to gravitational instability of the mantle lithosphere and lower crust) and velocity boundary condition (which simulates plate-motion forcing).

The work is intended to provide a framework that assists in interpreting the evolution of the active continental lithosphere. Conditions in the experiments span regimes that may characterize ancient to modern tectonic environments, and in this regard relate to various transects of the Lithoprobe project.

Method

The numerical experiments use the SOPALE code developed by Philippe Fullsack. The code uses an arbitrary Lagrangian-Eulerian (ALE) finite element method to solve for the creeping deformation of viscous-plastic materials assuming incompressibility and no inertial accelerations (Fullsack 1995). The governing equations for conservation of mass, momentum, and energy are

$$[1] \qquad \nabla \cdot \boldsymbol{u} = 0$$

$$[2] \qquad \nabla \cdot \sigma'_{ij} - \nabla p + \rho g = 0$$

$$[3] \qquad \rho c_p \left(\frac{\partial T}{\partial t} + \boldsymbol{u} \cdot \nabla T\right) = k\nabla^2 T + A$$

ρ, $\boldsymbol{u}$, p, and T represent the fields of density, velocity, pressure, and temperature; g, c_p, k, A, and t are gravitational acceleration, heat capacity, thermal conductivity, radioactive heat production (per unit mass), and time; and σ'_{ij} is the deviatoric stress tensor. Density is a function of temperature:

$$[4] \qquad \rho = \rho_0[(1 - \alpha(T - T_0)].$$

where α is the coefficient of thermal expansivity, ρ_0 is the reference material density, and T_0 is the reference temperature.

For the viscous-plastic formulation, the deviatoric stress is determined at each computational node as the lesser value of either a plastic yield stress σ_y or viscous stress σ_v. For the frictional plastic yield stress a Coulomb criterion is used:

$$[5] \qquad \sigma_y = \rho \sin\phi + c_0$$

where ϕ and c_0 represent the internal angle of friction and the cohesion, respectively. The viscous stress is defined as

$$[6] \qquad \sigma_v = 2\eta_e \dot{\epsilon}$$

where $\dot{\epsilon}$ is the second invariant of the strain rate and the effective viscosity η_e in this expression is

$$[7] \qquad \eta_e(\dot{\epsilon}, T) = \left(3^{\frac{-(n+1)}{2n}} 2^{\frac{1-n}{n}}\right) A^{\frac{-1}{n}} \dot{\epsilon}^{\left(\frac{1}{n}-1\right)} e^{\frac{Q}{nRT}}$$

The variables A, n, and Q are the viscosity parameter, power exponent, and activation energy from uniaxial laboratory experiments, and R is the ideal gas constant. (Note that the first bracketed term on the right hand side of eq. [7] is necessary for the conversion of the uniaxial laboratory experimental data to a state of stress that is independent of the choice of coordinate system.) Physical constants in the models are $\alpha = 2 \times 10^{-5}$ K^{-1}, $T_0 = 750$ K, g = 10.0 m/s^2, C_p = 750 J/kg/K, $\kappa = 1.0 \times 10^{-6}$ m^2/s, and $R = 8.31$ J/mol/K. In all the experiments, we ignore the effects of shear heating and radioactive heat production ($A = 0$ mW/m^3) in the energy equation (eq. [3]). Instead, the initial geotherms were designed to take into account radioactive heat production in the thermal structure of the crust and mantle lithosphere. The experiments consider the relatively short tectonic time scales (<100 million years) so that additional heating through radioactive decay is secondary compared with the advected heat in these active tectonic regions.

The ALE technique is particularly useful for our coupled crust–mantle models, since it can treat high strain of materials (e.g., the convecting mantle), and to track explicitly internal element deformation (e.g., that characterize lithospheric tectonics) and material interfaces (e.g., surface topography and internal boundaries). In the models, we use a free top surface so that topography can develop in response to the underlying dynamics.

We note that the set-up of these suites of models do not take into account an earlier phase of ocean plate subduction. Such a precursor event can modify the thermal characteristics of the lithosphere and, consequently, its propensity for deformation. However, to avoid adding a poorly constrained initial condition to the models, we assume that any such "continental back arc" is closed up or was not there to begin with, as in the continental collision at South Island, New Zealand.

Results

Continental collision

Even the fundamental style of evolution of the mantle lithosphere during continent–continent plate collision is not well understood. It has been proposed that during convergence, the mantle lithosphere is accommodated by distributed lithospheric thickening followed by convective removal of a viscous sub-crustal root (Houseman et al. 1981). In such models, the lower part of a dense thickened lithosphere (e.g., in a convergent zone) is gravitationally unstable and may develop as a viscous Rayleigh-Taylor-type mantle downwelling. It has been interpreted that the absence of a portion of the lithosphere and uplift at the Tibetan Plateau are a result of viscous instability and removal of the mantle lithosphere (England and Houseman 1989). Rayleigh-Taylor instability of the lithosphere has been well-studied with work considering how the process is modified by rheology (Buck and Toksöz 1983; Lenardic and Kaula 1995; Houseman and Molnar 1997; Molnar et al. 1998), shortening (Conrad and Molnar 1997; Molnar et al. 1998), and stratification (Neil and Houseman 1999; Houseman et al. 2000) of the lithosphere. As an example of an active continent collision, geophysical data have been interpreted to show that mantle lithosphere beneath South Island, New Zealand contains an approximately symmetric feature centred beneath the collision zone (Molnar et al. 1999; Stern et al. 2000). The inference is that this feature represents the descending viscous mantle lithosphere root beneath the crustal orogen.

Alternatively, it has been postulated that convergent continental mantle lithosphere may be accommodated by underthrusting of one plate beneath the other along a narrow shear zone in a subduction-like manner. The concept of subduction-style behavior of the mantle lithosphere has been incorporated as a basal boundary condition to drive crustal-scale models of compressional orogens (Willett et al. 1993; Beaumont et al. 1996). These studies demonstrate that for certain tectonic regimes a mantle subduction basal boundary condition is favored over a distributed Rayleigh-Taylor-type instability of the mantle lithosphere, as the former produces a distinct asymmetry in the crustal deformation, which is observed in many collisional orogens. Analyses of strain rate data derived from geodetic studies for the same South Island collision indicates that the width of crustal deformation is quite narrow — $<\sim 100$ km (Ellis et al. 2006). The interpretation is that this lends credence to the idea of localized mantle lithosphere deformation like subduction, rather than diffuse viscous instability.

Experiment set C sets up collision between two opposing continental plates (Fig. 2). It has no pre-existing perturbation of the mantle lithosphere, which is usually used to initiate Rayleigh-Taylor instability. Nor is there a velocity singularity (e.g., S-point) internal to the model to promote subduc-

Fig. 2. Illustration of the setup of the convergence "C" experiments. Crust, mantle lithosphere, and mantle regions are coloured differently as zones tracked in the models. The number of node points in the horizontal and vertical directions for the Eulerian and Lagrangian grids indicate resolution for the finite element mesh of quadrilateral elements. The numerical resolution is significantly higher in the upper portion of the model to better resolve the lithospheric deformation that develops in the experiments. The notation for strain weakening internal angle of friction ϕ means that ϕ decreases linearly from the maximum to minimum value across the strain range that is denoted. The retro- and pro- sides of lithosphere are denoted and a box with dashed outline depicts approximate portion of the full solution space that is shown in subsequent figures. The frame in the lower right shows the initial geotherm for the model. ϵ, the strain (specifically the square root of the second invariant of the deviatoric strain).

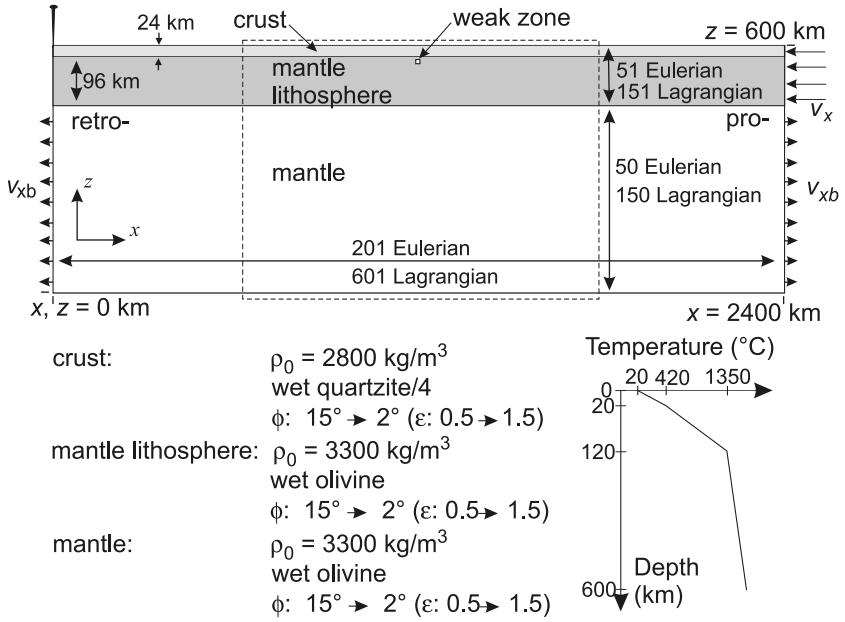

tion-like behaviour. Rather, all deformation in the model is driven by a combination of buoyancy forces (arising from thermal and inherent chemical density variations) and plate motions imposed at the boundary. Plate motion is simulated by introducing new lithosphere into the box at a horizontal velocity v_x = 1.5 cm/year at the right boundary of the model (Fig. 2). The left margin of the lithosphere is held fixed and a small outward flux, v_{xb} is distributed evenly along the sides of the sub-lithospheric upper mantle to balance the mass of injected lithosphere. The bottom boundary is free slip (i.e., zero normal velocity, zero tangential stress). A small weak "seed" is emplaced in the mantle lithosphere to locate the deformation at the centre of the box in the model, but otherwise this does not have an influence on the evolution of the model. The implicit assumption is that weak zones exist at plate boundaries.

The power-law viscous parameters (eq. [7] of the crust and mantle materials are based on experiments on the rheology of power-law creep. The viscous parameters of the mantle are based on a wet Åheim dunite with $A = 5.495 \times 10^{-25}$ Pa$^{-4.48}$/s, n = 4.48, Q = 498 kJ/mol (Chopra and Paterson 1984). For the crust, we assume a wet quartzite flow law with $A = 1.1 \times 10^{-28}$ Pa^{-4}/s, n = 4.0, Q = 223 kJ/mol (Gleason and Tullis 1995) but weakened by a factor of four. This crustal rheology is used to allow the lowermost crust to weaken sufficiently and develop some degree of crustal detachment from the underlying mantle. The chosen factor of 0.25 is somewhat arbitrary, being derived from observation of a series of numerical models (Pysklywec et al. 2002). However, it may be reasonable given the relatively high uncertainty in constraining wet material rheologies at depth, particularly the range of measured A values (eq. [7], the approximation of a purely quartzite controlled rheology, and the associated uncertainties in lithospheric temperatures.

Strain weakening of the materials is included within the frictional plastic component (eq. [5] of the material rheology (Fig. 2). Both mantle and mantle lithosphere are assigned the same rheological parameters and reference density, but they are differentiated by temperature. We define the lithosphere as mantle material having temperature <1300 °C. The initial geotherm for the experiments (Fig. 2) is laterally uniform and is defined by a fixed surface temperature of 20 °C and a series of underlying linear gradient segments to the bottom of the solution space: an increase to 420 °C at the base of the crust, to 1350 °C at a depth of 120 km, and to the bottom of the model, where the temperature is constant at 1500 °C.

In experiment C1, the first 166 km of shortening (in 11 million years) is accommodated by underthrusting of the pro-side of the mantle lithosphere beneath the retro-side at the collision zone along a well-developed shear zone (Fig. 3*a*). The upper portion of the mantle lithosphere is essentially "plate-like", and deformation of the Lagrangian mesh suggests that the plate-like region comprises the top ~70 km of the mantle lithosphere. There is evidence of increasing horizontal shear in the grid in the lower regions. This is a consequence of the viscous instability of the lowermost (warmest) portion of the thickened mantle lithosphere

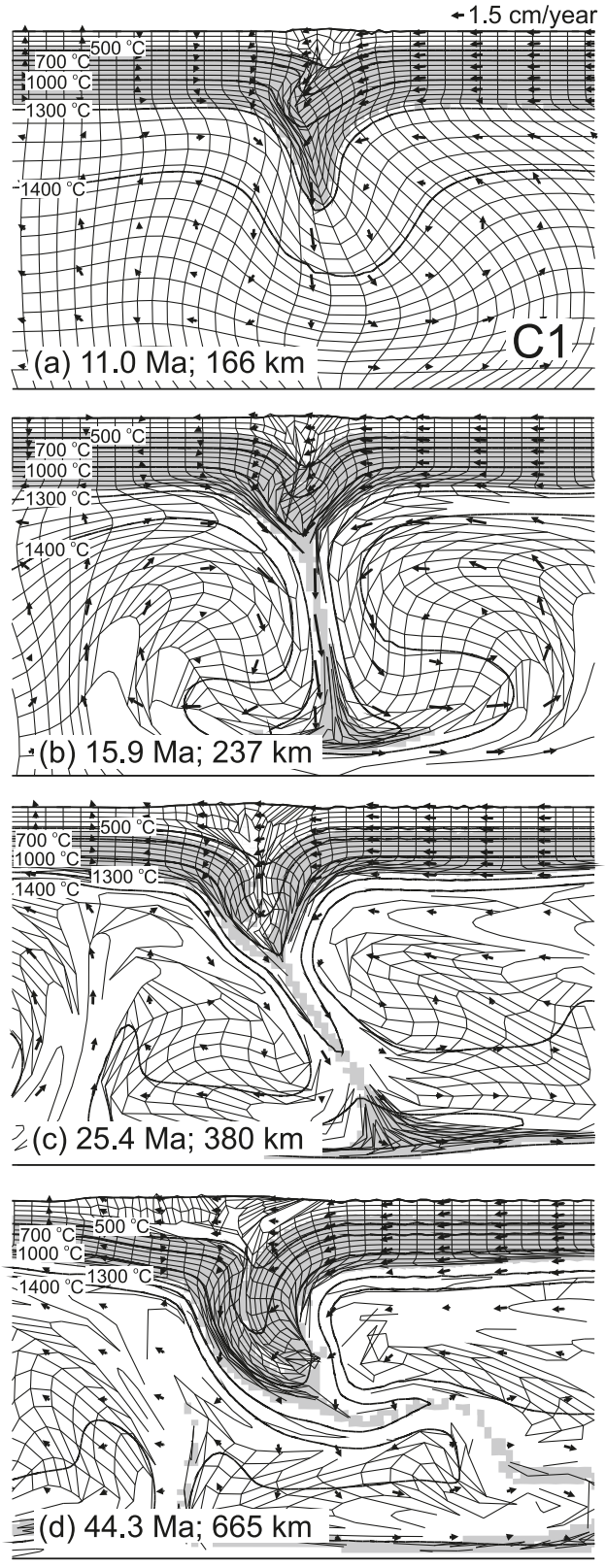

Fig. 3. Evolution of experiment C1 at indicated times and amounts of imposed convergence. Mantle lithosphere domain is shaded grey. The Lagrangian mesh (initially composed of rectangular cells) at one sixth (in *x*-direction) and one tenth (in *z*-direction) the actual resolution. Instantaneous velocity vectors and selected temperature contours are superimposed. Only a portion of the full numerical solution space is shown (see Fig. 2). For frame (*d*) the zoom box has been shifted to the left by ~150 km to bring the advanced collision towards the centre.

root, which is descending at ~4 cm/year. Above the mantle lithosphere, there is thickening and deformation of the crustal layer as an asymmetric wedge forms at the collision zone.

By 237 km of shortening (15.9 million years), the viscous instability "drips" into the mantle lithosphere at rates approaching 8 cm/year (Fig. 3*b*). This outpaces the convergent plate-like portion that still converges at 1.5 cm/year and underthrusts–subducts beneath the retro-side. The underthrusting–subduction progresses in a somewhat inhibited manner as the collision interface in the mantle lithosphere steepens. In certain models the retro-plate can act as an indenter at this stage leading to detachment and descent of the subducting pro-limb (Pysklywec et al. 2000; Pysklywec 2001). In turn, this effectively results in a reversal of the underthrusting–subduction polarity. We emphasise that only a portion of the full computational space is shown in Fig. 3 (and the other modeling figures). A series of secondary flow cells in the sub-lithospheric mantle away from the main descending lithosphere suggest that the box side boundaries are not influencing the main lithospheric deformation.

The plate steepening develops into an ablative, almost symmetric type of plate consumption (Tao and O'Connell 1992) by 380 km of convergence (Fig. 3*c*). That is, the retro- and pro-plates are essentially equally consumed. In this experiment, the downgoing mantle lithosphere does not remain plate-like to significant depth, but rather after reaching ~200 km, it is sufficiently hot and low viscosity to drip through the upper mantle. The progressive rapid dripping of mantle lithosphere induces vigorous return flow and advection of high mantle temperatures towards the surface. By this stage of the experiment, a wider wedge of thickened crust — reaching ~50 km — has formed.

At 665 km of shortening (44.3 million years), the mantle lithosphere collision and crustal deformation front have migrated a significant distance retro-ward (Fig. 3*d*). Furthermore, a distinct asymmetry has redeveloped. The crustal orogen has highly localized deformation on the pro-side of the wedge whereas lateral growth, distributed thickening, and a plateau-type uplift characterize the retro-side. Although the underlying mantle lithosphere behaviour is effectively a two-sided plate consumption, the process is not symmetric at the crustal scale. The pro-mantle lithosphere remains at its nominal depth, meaning it is still cool, strong, and behaves generally plate-like. The retro-lithosphere is thickening and remains strong and plate-like as cold isotherms are advected downwards.

This model is consistent with other series of experiments that we have run for generic collisional events (Pysklywec et al. 2000; Pysklywec 2001) and continental convergence at South Island, New Zealand (Pysklywec et al. 2002). A robust feature is that during the initial stages of plate collision, it is difficult to define one specific deformational style for the system, but instead it can be characterized by contemporaneous, but distinct processes of crustal thickening, underthrusting–subduction of the upper plate-like portion of the

Fig. 4. Evolution of experiment C2 at indicated times and amounts of imposed convergence. This model is identical to C1, except the convergence rate (and outgoing boundary flux) has been tripled. Mantle lithosphere domain is shaded grey. The Lagrangian mesh (initially composed of rectangular cells) at one sixth (in *x*-direction) and one tenth (in *z*-direction) the actual resolution. Instantaneous velocity vectors and selected temperature contours are superimposed. Only a portion of the full numerical solution space is shown (see Fig. 2).

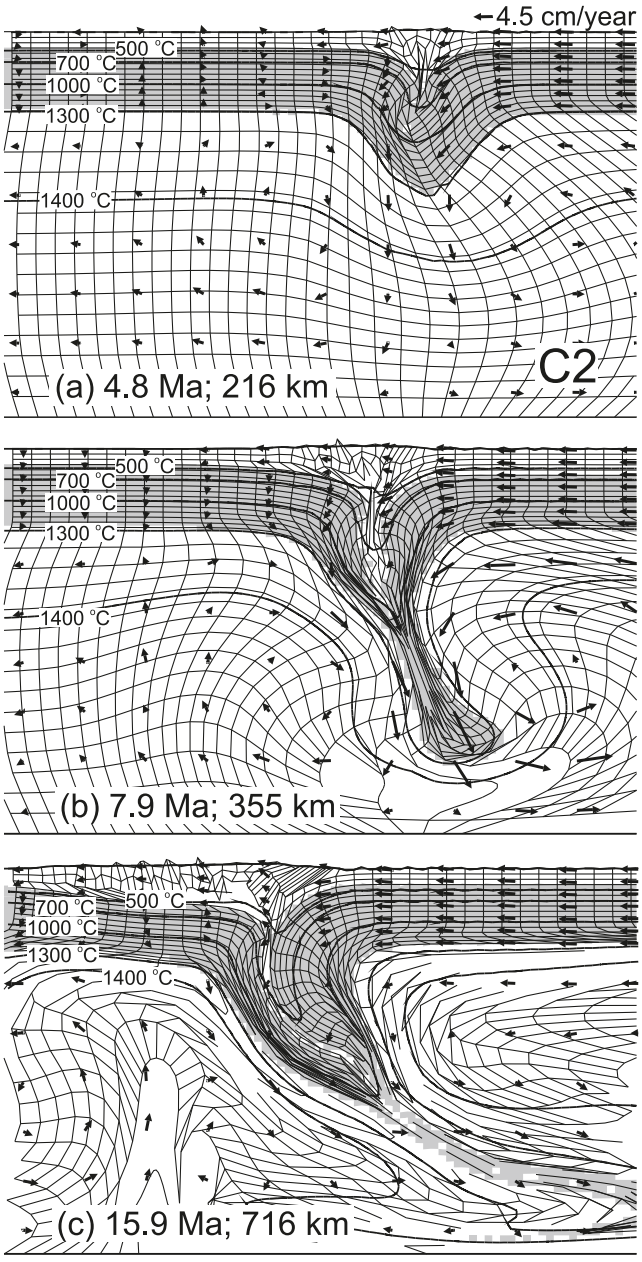

mantle lithosphere, and viscous instability of the lower lithosphere. Subsequently, "clean" subduction behaviour does not occur. Instead, with warming of the convergent lithosphere transitions to a less plate-like character, leading to steepening, dual-sided consumption, and viscous dripping into the mantle.

With this type of mixed- or transitory-mode of deformation the crust deforms in a manner governed by the generally subduction-like behaviour of the uppermost mantle lithosphere. As a result, it is consistent with observations of asymmetric orogens with spatially localized deformation (Beaumont et al. 1996; Ellis et al. 2006). However, the lower part of the mantle lithosphere can be in transition to a non-plate like behaviour that modifies the gross structure of the lithosphere. This may account for observations and interpretations of the large-scale structure of convergent mantle lithosphere (Stern et al. 2000).

Previous models show that plate convergence rate controls geodynamical evolution since material rheology is modified by changing rates of deformation, and convergence governs the relative rate of plate boundary and gravitational forcing (Pysklywec et al. 2000, 2002; Pysklywec 2001). With convergence velocity tripled to 4.5 cm/year the model is similar but the relative timing of the tectonic events change (experiment C2; Fig. 4). There is initial subduction–underthrusting of the pro-plate mantle lithosphere. However, the dripping behaviour of the lowermost lithosphere is less pronounced since plate convergence is high enough to keep up with the growth rate of any viscous instability (Fig. 4*a*). The mantle lithosphere collision again steepens into an ablative-type collision (Fig. 4*b*). The front of the consumed lithosphere tends to drip as it protrudes mid-way through the warm and vigorously overturning upper mantle.

As in C1, the consumption and especially the crustal deformation shifts back to an asymmetric geometry at mature stages of the model (Fig. 4*c*). The pro-side of the crust and mantle lithosphere are well coupled, whereas in the hotter retro-side, there is less coupling between these two regions. The deformation front advances rapidly with the higher convergence rate, migrating $\sim$400 km in the retro-ward direction in 16 million years.

Mantle lithosphere rheology represents a first-order control on the behaviour of the lithosphere during convergence. Substitution of a dry olivine flow law (Hirth and Kohlstedt 1996) for mantle lithosphere reduces the propensity for the mantle lithosphere to develop viscous gravitational instabilities (Pysklywec et al. 2002). Alternatively, the wet olivine flow law of Hirth and Kohlstedt (1996) with $A = 4.89 \times 10^{-15}$ Pa$^{-3.5}$/s, $n = 3.5$, $Q = 515$ kJ/mol results in a weaker viscous and, hence, more unstable mantle lithosphere than that of Chopra and Paterson (1984) and Pysklywec et al. (2002). For example, using a strain rate of 10^{-15} s^{-1} and temperature of 1600 K, the former is a factor eight times lower viscosity than the latter based on eq. [7].

Collision experiment C3 is the same as C1, but the viscosity of the mantle lithosphere is scaled higher by a factor of 10 (Fig. 5). In this instance, subduction-like consumption of the convergent pro-plate is dominant. At 12.7 million years (190 km convergence), the pro-mantle lithosphere underthrusts the retro-side at a shallower angle than either C1 or C2. This continues through 28.5 million years (428 km) as the pro-mantle lithosphere subducts to a depth of $\sim$350 km along a well-developed shear zone. The lower mantle lithosphere has a high enough viscosity that it tends not to drip into the mantle; only the very leading portion of the subducted plate warms and drips downward (Fig. 5*b*). As a result, there is less sub-lithospheric mantle flow (induced by the lithospheric motion) in C3 in comparison with the previous models. By 42.2 million years (618 km), the retro-mantle

Fig. 5. Evolution of experiment C3 at indicated times and amounts of imposed convergence. This model is identical to C1, except the viscosity of the mantle lithosphere has been increased by a factor of 10. Mantle lithosphere domain is shaded grey. The Lagrangian mesh (initially composed of rectangular cells) at one sixth (in *x*-direction) and one tenth (in *z*-direction) the actual resolution. Instantaneous velocity vectors and selected temperature contours are superimposed. Only a portion of the full numerical solution space is shown (see Fig. 2).

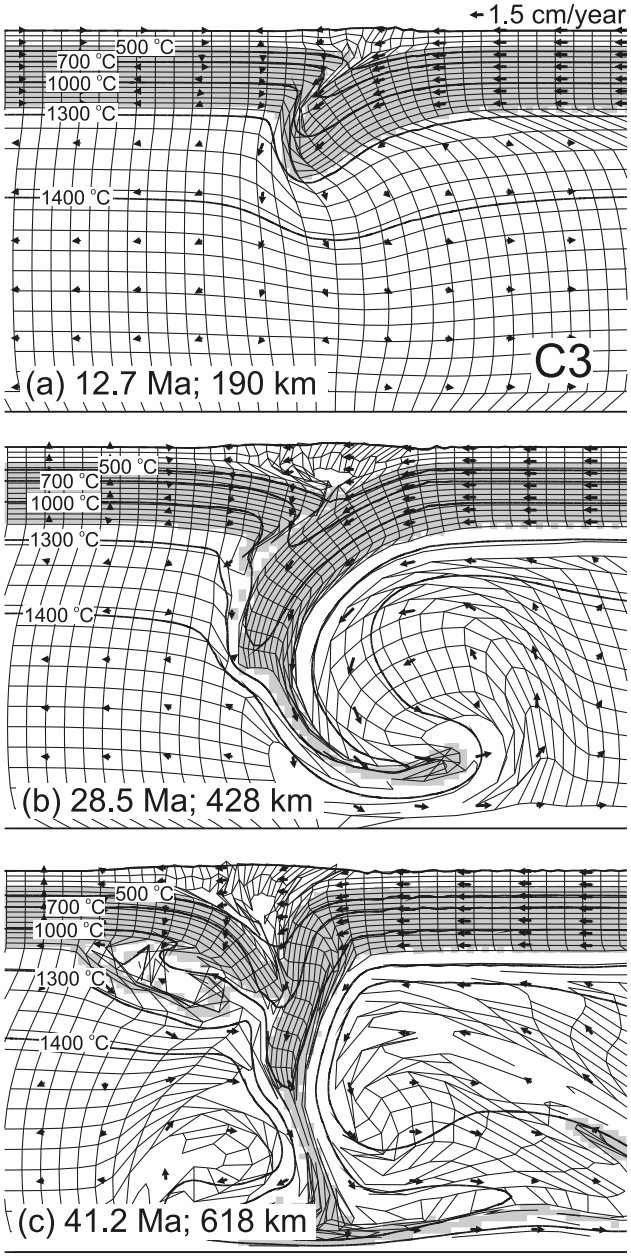

Fig. 6. Evolution of experiment C4 at indicated times and amounts of imposed convergence. This model is identical to C1, except surface erosion has been imposed at the surface, as described in the text. Mantle lithosphere domain is shaded grey. The Lagrangian mesh (initially composed of rectangular cells) at one sixth (in *x*-direction) and one tenth (in *z*-direction) the actual resolution. Instantaneous velocity vectors and selected temperature contours are superimposed. Only a portion of the full numerical solution space is shown (see Fig. 2).

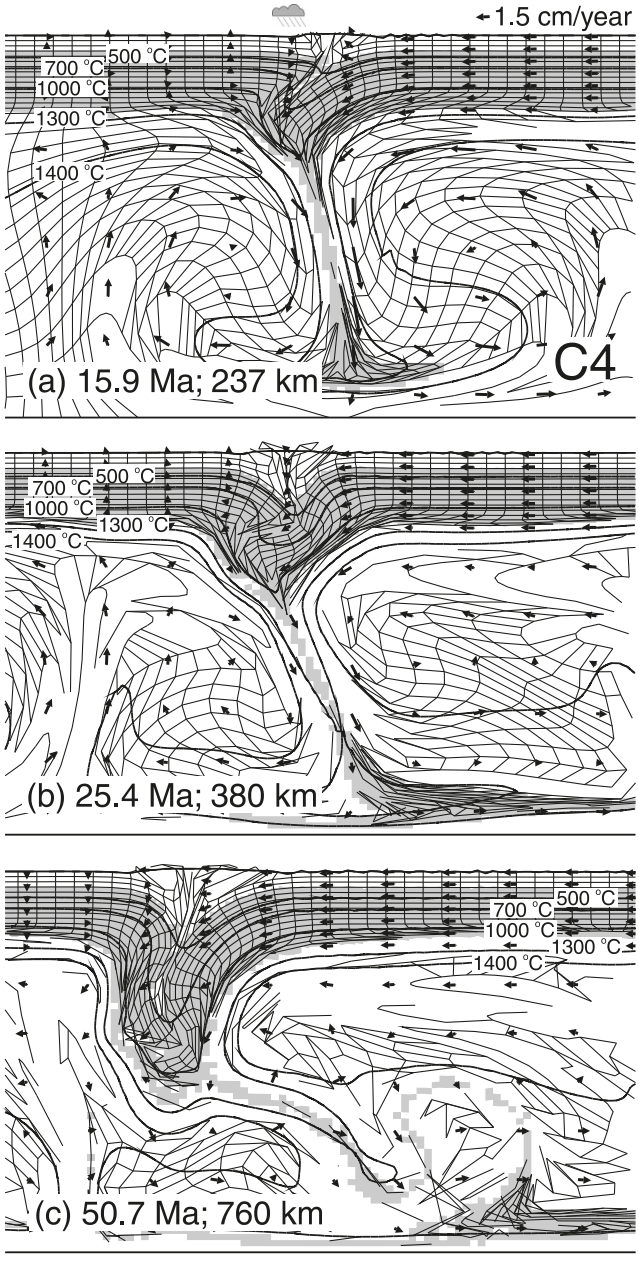

lithosphere indents the pro-side and the clean subduction behaviour is broken. Rather than causing slab detachment and reversal of consumption polarity as discussed earlier in the text, the experiment evolves to another two-sided consumption of both the pro- and retro-mantle lithosphere.

Modified crustal rheologies have not been considered in the models. A large part of the crustal behaviour is controlled by its brittle-frictional properties (eq. [5]), including the imposed strain softening, which is poorly constrained. A model with a higher initial geotherm (increased by 11%) shows how a weakening of the thermally activated viscosity of the crust and mantle lithosphere modifies the plate behaviour (experiment EX6; Pysklywec et al. 2002). In this case, the gravitational instability in the lower mantle develops on a significantly shorter time scale than in the other experiments. The upper portions of the mantle lithosphere and

crust is still governed by the brittle-frictional rheology, meaning a subduction-like underthrusting of one side beneath the other as in C1.

Collision and surface erosion

The influence of surface erosion and deposition is not included in the previous experiments. Crustal-scale models of collision and orogenesis have demonstrated that the internal structure, morphology, and thermal evolution of the crust may be strongly modifed by erosion (Beaumont et al. 1992; Koons 1995; Batt and Braun 1997; Willett 1999). Upper mantle-scale modeling suggests that the influence of surface erosion may extend below the crust to modify the behaviour of the mantle component of the lithosphere (Pysklywec 2006). Experiment C4 demonstrates this by imposing surface erosion to a configuration identical to C1. Based on Montgomery and Brandon (2002), an empirical law for erosion rate E in tectonically active orogens is used:

$$[8] \qquad E = E_0 + \frac{kR_z}{1 - (R_z/R_c)^2}$$

where $k = 2.5 \times 10^{-4}$ year^{-1} is a proportionality constant, $E_0 = 0.01$ mm/year is the background erosion rate due to chemical weathering, R_z is local relief (taken as the top free surface of the numerical grid), and $R_c = 1500$ m is a limiting local relief. As with the other models, the convergent promantle lithosphere is initially consumed in subduction-like manner (15.9 million years, 237 km; Fig. 6*a*). We do not focus on the crust here, but the inclusion of erosion promotes strain localization within the crustal orogenic wedge (e.g., Beaumont et al. 1996). It is interesting to compare this relatively coherent subduction with the same stage in experiment C1. There, the retro-plate is starting to indent the proplate and steepening (Fig. 3*b*). The difference between the erosion and non-erosion model becomes more marked by 25.4 million years (380 km). With erosion in C4, the proplate is still underthrusting the retro-plate, although the latter is starting to indent and break the former (Fig. 6*b*). In the absence of erosion (C1), well-developed two-sided plate consumption occurs (Fig. 3*c*). In line with previous studies (Pysklywec 2006), these results indicate that the modification of crustal mass flux by surface erosion can change the dynamics at the crust–mantle interface and consequently alter the response of the mantle lithosphere. Essentially, with active surface erosion, stable subduction-like consumption of mantle lithosphere is maintained; in the absence of erosion, mantle lithosphere subduction tends to be inhibited by accumulating crust. Depending on lithospheric rheology, density, and plate velocity, the differences between non-erosion and erosion models can be more pronounced, even with the potential to trigger delamination or retreat of the convergent plate (Pysklywec 2006).

As convergence progresses in experiment C4, the mantle lithosphere eventually evolves toward two-sided consumption (Fig. 6*c*). In contrast to C1, however, the mantle lithosphere and crust are well coupled on both the retro- and prosides of the collision. This is a consequence of the sustained localization of crustal thickening by the surface erosion. Variations in the direction and magnitude of erosion will modify the crustal orogenesis (Willett 1999) and underlying mantle lithosphere behaviour, but the experiment demonstrates how surface erosion can modify the evolution of the deepest part of the lithospheric plate.

Detachment of subducted–underthrust mantle lithosphere does not manifest in these series of convergence experiments. Such behaviour does occur in certain models, and is controlled in part by the yield strength rheology of the mantle lithosphere and its density contrast with the underlying mantle (Pysklywec et al. 2000; Pysklywec 2001). Seismic tomographic inversions have been interpreted to image fragments of Tethyan oceanic and Indian continental lithosphere beneath the India–Eurasia collision (Van der Voo et al. 1999). Such plate detachment can have some notable consequences. Subduction polarity reversal may follow from the detachment and such a mechanism has been invoked to account for the flip in subduction polarity across Taiwan (Teng et al. 2000; Pysklywec 2001). In addition, detachment of subducted continental mantle lithosphere may lead to a rapid surface uplift as the dense lithospheric load is removed from the remaining lithosphere (Buiter et al. 2001).

Mantle lithosphere removal

In the preceding instances of continental collision, there is accretion and thickening of mantle lithosphere. However, geological, geophysical, and geochemical evidence identifies several locations at or near plate boundaries or within plate interiors where a significant portion or all of the continental mantle lithosphere may be absent. A type example is in the Southern Sierra Nevada, where it has been interpreted that up to 85% of the mantle component of the lithosphere is missing (Wernicke et al. 1996; Meissner and Mooney 1998; Lee et al. 2000; Saleeby et al. 2003; Zandt et al. 2004). Removal of mantle lithosphere has also been postulated beneath the Alboran Sea Rif-Betics (Platt and Vissers 1989; Seber et al. 1996), eastern Anatolia (Keskin 2003; Sengör et al. 2003; Göğüs and Pysklywec 2008*b*), central Andes (Kay and Kay 1993), and Tibet (England and Houseman 1989; Chen and Tseng 2007), among other regions.

There are two primary mechanisms that have been put forward to account for mantle lithosphere removal. It may be that mantle lithosphere is removed by Rayleigh-Taylor-type viscous instability (“dripping”) of the cold dense lithosphere (Houseman et al. 1981). Alternatively, the cold and dense mantle lithosphere may peel away as a coherent slice from the crust along the Moho — i.e., delamination as proposed by Bird (1979). This involves separation between strong crust and strong mantle lithosphere portions of the plate where the hot, weak lower crust is a pronounced lithospheric strength discontinuity. As described in the prior section, the process of viscous gravitational instability of the lithosphere has been quite well studied. There has been less focus on delamination, but recent work provides insight into the conditions and consequences of it (e.g., Morency and Doin 2004; Sobolev and Babeyko 2005; Pourhiet et al. 2006; Göğüs and Pysklywec 2008*a*, 2008*b*). Such mantle lithosphere removal events are predicated on the density contrast of the cold mantle lithosphere with respect to the warmer less dense underlying mantle. As such, gravity is the controlling driving force on the mantle lithosphere tectonics, rather than plate convergence.

The emphasis of our work has been to study the relationship between the sub-crustal removal events and the evolu-

Fig. 7. Illustration of the setup of the convergence "D" experiments. Crust, mantle lithosphere, and mantle regions are shaded differently as zones tracked in the models. The number of node points in the horizontal and vertical directions for the Eulerian and Lagrangian grids indicate resolution for the finite element mesh of quadrilateral elements. The numerical resolution is significantly higher in the upper portion of the model to better resolve the lithospheric deformation that develops in the experiments. The notation for strain weakening internal angle of friction ϕ means that ϕ decreases linearly from the maximum to minimum value across the strain range that is denoted.

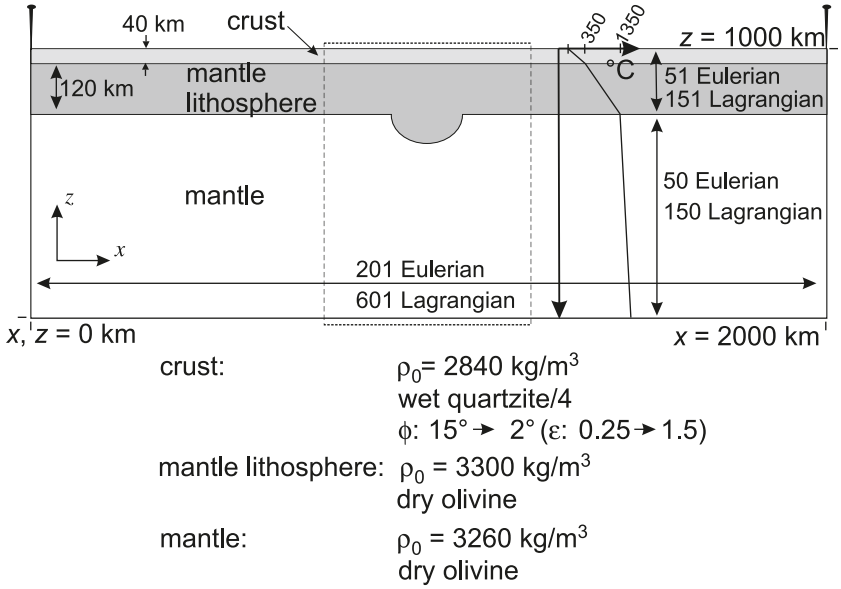

tion of the crust. Specifically, we consider the topographic, thermal, and structural–deformational expression of the crust to delamination and drip-type viscous removal of the mantle lithosphere. The models demonstrate how mantle flow drives crustal tectonics, but more specifically are meant to help interpret lithospheric dynamics (e.g., "drip" or "delamination") from surface observables.

Numerical models of dripping lithospheric removal

The set-up of the D-series of experiments for mantle lithosphere removal is shown in Fig. 7. It is broadly similar to the C model configuration except that for the D experiments no plate convergence is imposed. Although we recognise that many of the removal events occur in convergent zones, we are trying to isolate the dynamics of the gravity-driven flow. For the mantle rheology, we now use a dry olivine flow law based on the experimental results of Hirth and Kohlstedt (1996); i.e., $A = 4.85 \times 10^{-17}$ Pa$^{-3.5}$/s, $n = 3.5$, $Q = 535$ kJ/mol. A somewhat arbitrary 50 km radius hemispherical perturbation of mantle lithosphere material is added at the base of the lithosphere to initiate viscous instability of the lithosphere. The size of this dense anomaly can change the growth rate of the instability (Houseman and Molnar 1997), but we only examine one size of perturbation in the experiments presented here.

The top of the solution space is a free surface, while free slip boundary conditions (i.e., zero normal velocity, zero tangential stress) are imposed on all other faces. The initial temperature profile has the top boundary of the box held at 20 °C and the bottom boundary at 1500 °C (Fig. 7); heat flux across the side boundaries is zero. The 350 °C Moho is based on estimates for the southern Sierra Nevada of California (Lachenbruch and Sass 1977), as a region where both dripping and delamination have been postulated.

In experiment D1, the gravitationally unstable mantle lithosphere drips over the first 12.6 million years (Figs. 8*a*, 8*b*). Inspection of the Lagrangian mesh indicates that it is primarily the lowermost portion of the mantle lithosphere that is participating in the downwelling. Initially, the colder, stronger upper mantle lithosphere is only mildly deformed as the lower part flows downward (Fig. 8*b*). The drip downwelling eventually causes significant horizontal entrainment with surrounding mantle lithosphere being drawn towards the centre of the box at the removal zone. By the later stages (38 million years; Fig. 8*c*), even the upper mantle lithosphere and crust are affected by this horizontal entrainment. Consequently, there is crustal contraction directly above the mantle lithosphere instability. Note that while this downwelling and entrainment are active, the mantle lithosphere is not thinned at the unstable zone, but rather the removal occurs in the peripheral regions.

As an alternative experiment, D2 ignores the temperature dependent component of the viscous rheology of the mantle lithosphere. For eq. [7], we set $Q = 0$ and compensate by making $A = 10 \times 10^{-40}$ Pa$^{-3.5}$/s and $n = 3.5$. This results in a similar average effective viscosity of the mantle lithosphere in D2 to D1, although the former is temperature independent. Part of the motivation for this is to enable a numerical model with a similar behaviour to the physical analogue dripping experiments.

D2 shows rapid instability of the mantle lithosphere (Figs. 8*d*–8*f*). Minor perturbation starts by 3.8 million years, then a significant drip descends at 4.5 million years. As opposed to D1, the whole thickness of mantle lithosphere participates in the downwelling, but the viscous instability occurs over a smaller lateral extent. This is owing to the temperature-independence and strain rate-dependence of the mantle lithosphere rheology: the cold upper mantle litho-

Fig. 8. Evolution of experiments D1 and D2 at indicated times. This model is identical to C1, except surface erosion has been imposed at the surface, as described in the text. Mantle lithosphere domain is shaded grey. The Lagrangian mesh (initially composed of rectangular cells) at one sixth (in *x*-direction) and one tenth (in *z*-direction) the actual resolution. Instantaneous velocity vectors and selected temperature contours are superimposed. Only a portion of the full numerical solution space is shown (see Fig. 7).

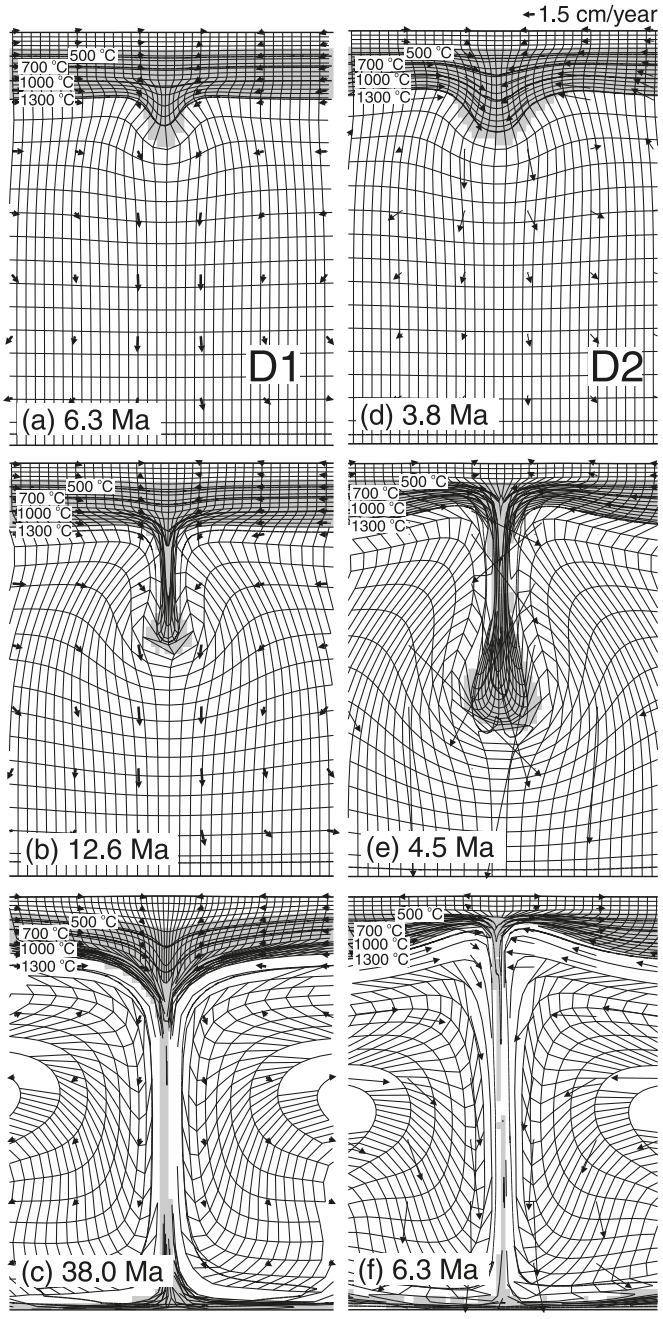

sphere is no stronger than the lower mantle lithosphere and the strain-rate weakening results in a more localized instability. The removal in D2 involves less horizontal entrainment of surround mantle lithosphere. Rather, the localized descent of mantle lithosphere results in a ~400 km wide mantle lithosphere gap (Fig. 8*f*).

Tractions at the crust–mantle interface during mantle lithosphere removal induce deformation of the crust, thereby modifying Moho and surface topography. Figure 9 shows surface topography and silhouettes of the crust at two stages of D1. Initially, the surface (and Moho) subsides as a manifestation of dynamic topography associated with the dripping mantle lithosphere (Fig. 9*a*). By 38 million years, this inverts to a positive topography as the crust contracts and thickens and the consequent isostatic uplift overwhelms the on-going dynamic subsidence (Fig. 9*b*). The crust is entrained downwards by mantle flow to ~80 km depth and results in a steep embayment of crust into the mantle directly above the drip. Such a feature is similar in form to a "V-shaped" portion of crust intruding into the mantle lithosphere as interpreted from seismic surveys across the southern Sierra Nevada (Zandt et al. 2004).

For D2, there is a similar inversion from subsidence to uplift above the dripping mantle lithosphere, but the topography tends to be more localized above the centre of the downwelling (Fig. 10). More notably, there is significantly less entrainment of crust into the mantle than in D1. In D2, only a small wedge of crust is pulled into the mantle lithosphere and to a depth of 47 km (Fig. 10*b*). As discussed earlier in the text, the mantle lithosphere rheology of D2 results in less horizontal entrainment, and this is reflected in the crustal evolution.

This interplay between dynamic topography and flow-induced crustal deformation that controls the surface topography depends strongly on the rheology of the crust and mantle lithosphere (Fleitout and Froidevaux 1982; Marotta et al. 1999; Neil and Houseman 1999; Pysklywec and Shahnas 2003; Pysklywec and Cruden 2004). If the bulk crust is strong (e.g., $\eta_e > 2.5 \times 10^{25}$ Pa·s), it will resist internal deformation and will only experience surface deflections from mantle flow normal stresses. If there is a weak ductile lower crust beneath a strong upper crust, the mantle lithosphere removal can induce extreme deformation in the former region, while the latter remains relatively intact. The crustal viscosity of the D1 and D2 models lie somewhere between these very strong crust and weak lower crust end-members; accordingly they demonstrate a moderate crustal deformation induced by the mantle lithosphere downwelling.

The thermal signature of the mantle lithosphere removal on the crust is markedly different between the two experiments. Figure 11 shows the maximum temperature in the crust as a function of time. For D1, since only the lower part of the mantle lithosphere is involved in the rapid flow instability, the crust is rather well thermally insulated during this removal, rising only ~50 °C over the duration of the experiment. On the other hand, with (rapid) removal of most of the mantle lithosphere in D2, the peak crustal temperature spikes to 1150 °C at 12 million years. After this, temperature decreases as the mantle lithosphere gap and overlying crust cool.

The thermal properties of the crust may influence the development of mantle lithosphere removal. Numerical models of viscous instability suggest that the presence of radioactive elements (which was not included in the model sets shown here) may make otherwise strong crust vulnerable to intraplate tectonic deformation and represent a primary control on the way the strength of the crust evolves during sub-crus-

Fig. 9. Surface topography (right axis) and crust silhouette (left axis) for experiment D1 at selected times. The surface topography is essentially a zoomed plot of the top surface of the silhouette. Arrow indicates location of viscous instability at centre of box.

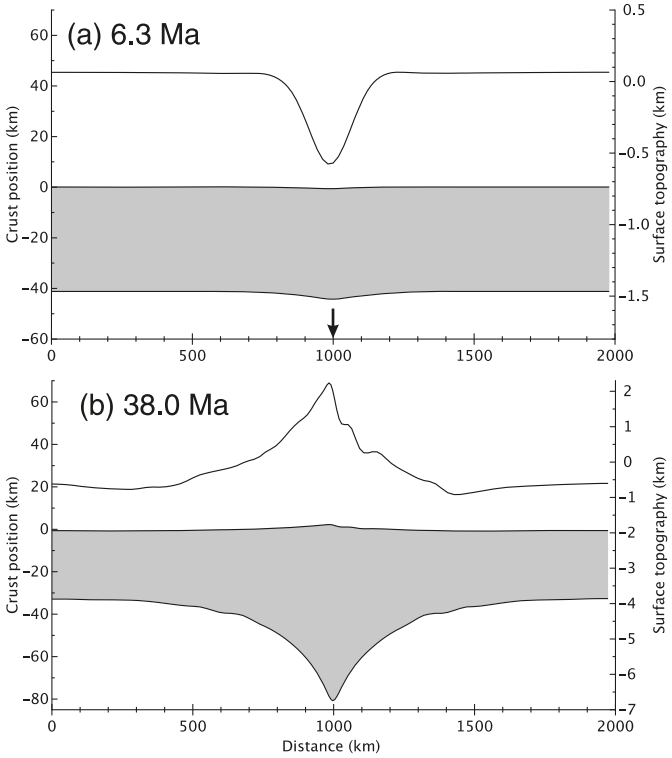

Fig. 10. Surface topography (right axis) and crust silhouette (left axis) for experiment D2 at selected times. The surface topography is essentially a zoomed plot of the top surface of the silhouette. Arrow indicates location of viscous instability at centre of box.

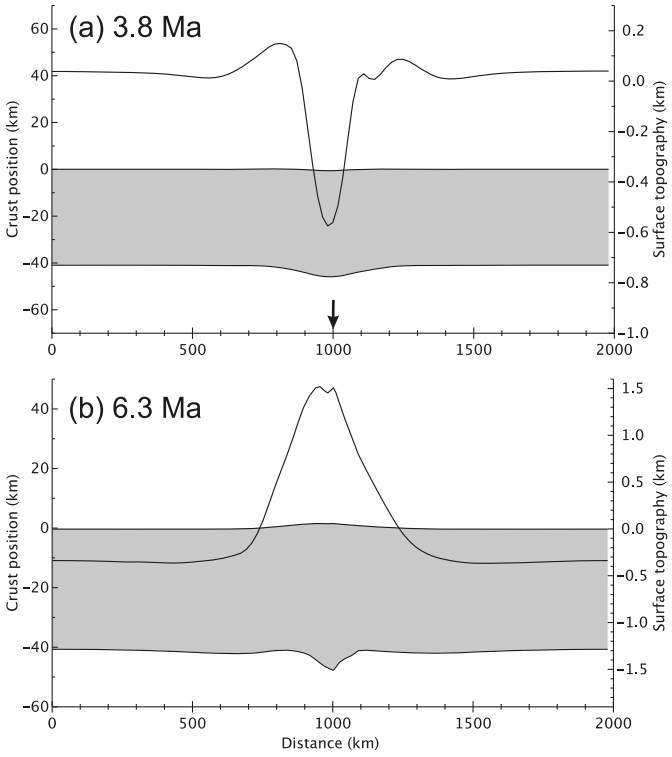

Fig. 11. Maximum temperature within the crust as a function of time for the three D experiments (D1, D2,and DE1). Note that the specific position of maximum temperature within the crust changes throughout the course of the experiments.

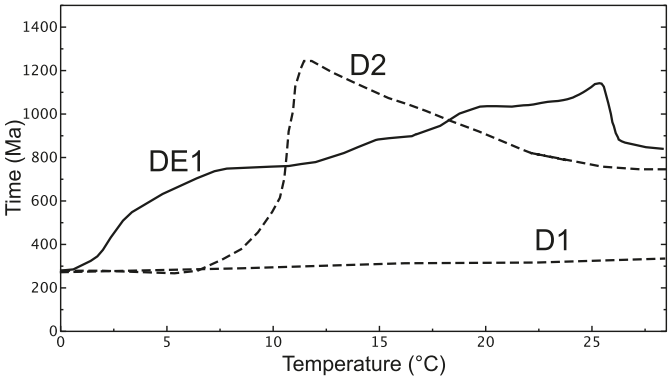

tal forcing (Pysklywec and Beaumont 2004). The models demonstrate a sequence of subsidence, contraction and uplift, and extension and crustal deflation that makes up an intraplate tectonic inversion event. Regions of high radioactive heat production and juvenile crust would be particularly prone to such processes. For example, the Mount Isa region of Australia represents a region of high past and present heat flow having a relative abundance of radioactive heat producing elements in its crust and since the Paleoproterozoic has experienced a number of episodes of intraplate tectonic activity (e.g., Shaw et al. 1991; O'Dea et al. 1997; Betts 1999; Scott et al. 2000). Consistent with the modeling, it has been proposed that there may be a causal relationship between the radioactive heating–weakening and certain phases of intracratonic deformation (Sandiford and Hand 1998; McLaren et al. 1999; McLaren and Sandiford 2001; Sandiford and McLaren 2002).

Scaled analogue models of dripping lithospheric removal

We have conducted many series of physical scaled analogue models of dripping-type mantle lithosphere removal in parallel with the computational models. The advantage of the analogue models is that they are three dimensional and can show detailed complex structural evolution of the crust in response to the mantle dynamics. Figure 12*a* shows a side view of the cylindrical modeling tank for experiment DA1, which introduces a small circular perturbation to the base of the dense mantle lithosphere. The mantle lithosphere material is a mix of polydimethylsiloxane (PDMS) and plasticene and underlies a ductile lower crust of PDMS, plasticene, and glass beads, and a brittle upper crust of ceramic microspheres. The remainder of the tank is filled with PDMS as the sub-lithospheric mantle. The densities and rheological parameters for these materials are listed in Table1. The viscous fluid mixtures have a slightly non-Newtonian rheology defined by the flow law:

$$[9] \qquad \sigma'^{n} = \eta\dot{\epsilon}$$

where σ is the deviatoric strain, n is the power exponent, $\dot{\epsilon}$ is the strain rate, η is the viscosity; and the microspheres are governed by a Coulomb behaviour (eq. [5].

Scaling of the experiment follows the approach for analogue modelling of lithospheric deformation at one-gravity

Fig. 12. Experiment DA1. (*a*) Schematic of the set-up for analogue drip model. See Table 1 for details of model properties and crustal thicknesses. (*b*) Side view of cylindrical tank immediately after initial construction. The upper crust is barely visible at the top above the beige lower crustal layer. (*c*) Side view photo of the experiment at 14 h. The "E" denotes the east side of the tank for reference in the subsequent frames. (*d*) Top view photo of the experiment at 14 h. Initially regular square marker grid on the top surface demonstrates deformation of upper crust. The small dark,red circular features that appear on the surface are caused by small air bubbles that rise and puncture through the crust during the experiment. These features cause only an aesthetic disturbance and have no influence on the general evolution of the experiments. (*e*) Oblique top view photo at the end of the experiment (23 h) after the granular upper crust has been vacuumed off. Solid line indicates the location of the cut section next frame. (*f*) Cut north–south section through the terminated model.

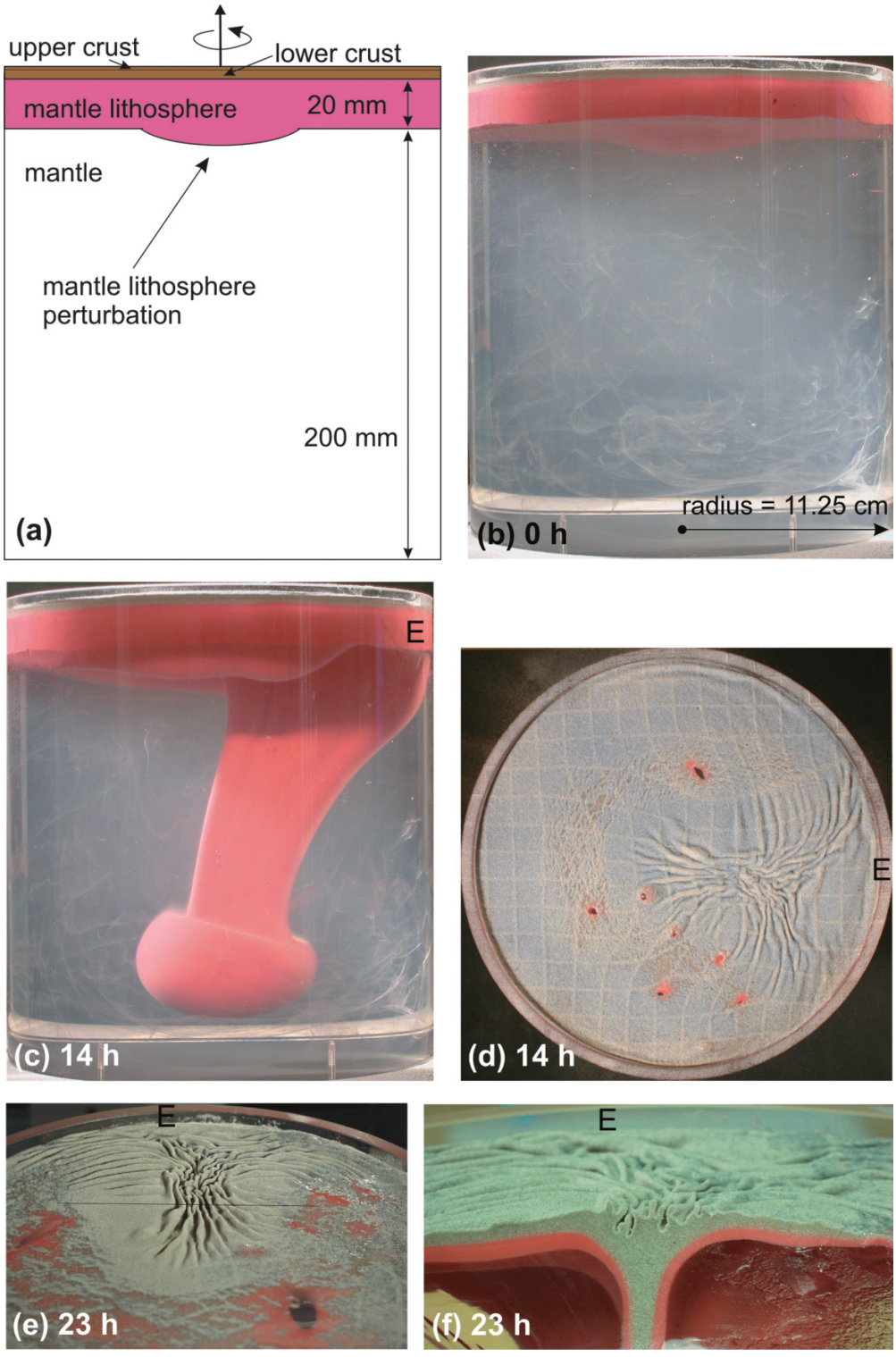

Table 1. List of experiments and associated modeling parameters (see text for definition of variables), with the values scaled to the natural system given in parentheses.

	Thickness	ρ (kg/m^3)	η (Pa·s)	n	ϕ	σ_0 (Pa)
Upper crust	2 mm	900	—	—	35°	10
	(12 km)	(2900)	—	—	(35°)	(1×10^6)
Lower crust	5 mm	930	5.0×10^4	1.1	—	—
	(29 km)	(3000)	(2×10^{21})	(1.1)	—	—
Mantle lithosphere	20 mm	1040	7.2×10^4	1.1	—	—
	(120 km)	(3300)	(3×10^{21})	(1.1)	—	—
Mantle	200 mm	960	2.5×10^4	1.1	—	—
	(1200 km)	(3100)	(1×10^{21})	(1.1)	—	—

(1g) described by Davy and Cobbold (1988, 1991). The experiments are approximately scaled to nature by selection of appropriate dimensions (geometric similarity) and laboratory materials (dynamic and kinematic similarity). We define a length scale based on a model lithospheric thickness, l_m = 2.0 cm, which for a natural continental lithospheric thickness l_p = 120 km gives a length scale ratio $L = l_m/L_p = 1.7 \times 10^{-7}$. A mantle density ρ_m = 960 kg/m^3 and a natural asthenospheric density of ρ_p = 3100 kg/m^3 sets a density scale of $P = \rho_m/\rho_p = 0.31$. For scaling purposes, we define an effective viscosity $\eta_{eff} = \sigma/\dot{\epsilon}$, which for PDMS at a laboratory strain rate of 10^{-5} s^{-1} is 2.5×10^4 Pa·s. Assuming an effective viscosity of $[\eta_{eff}]_p = 10^{21}$ Pa·s for the natural asthenosphere (Motrovica and Forte 1997) define a viscosity scale ratio $M = [\eta_{eff}]_m/[\eta_{eff}]_p = 2.5 \times 10^{-17}$. The scale ratio for gravitational acceleration is $G = g_m/g_p = 1$, so the time scale ratio for the experiments can now be defined as $T = M/\text{PLG} = t_m/t_p = 4.8 \times 10^{-10}$.

Compared with the numerical drip models, the geometry of the model is similar, with comparable crustal and mantle lithosphere thicknesses (Table 1). Density and viscosity in the analogue models are temperature independent, but model D2 was modified to take this into account by removing the (strong) dependence of viscosity on temperature. One of the main limitations of the analogue models is that the viscosity contrast between the lithosphere and underlying mantle is not very high (a factor of 3; Table 1) compared with that in the numerical models (up to a factor of 100). This is a consequence of limited specific materials available for simulating the sub-lithopheric mantle (e.g., with a proper power-law exponent and density).

By 14 h (scaled to 3.3 million years), the dense mantle lithosphere has dripped into the mantle as a plume-like feature, almost to the bottom of the tank (Fig. 12*b*). The instability has shifted to the east side of the tank. This type of migration of the locus of downwelling is something that occurs in most of the analogue experiments, although it may have to do with the relatively close lateral confinement of the flow tanks (Pysklywec and Cruden 2004).

The upper crustal deformation is illustrated by contortion of a coloured passive marker grid (initially square) dusted on the top surface (Fig. 12*c*). At 14 h, there is strong contraction above the drip characterized by a complex system of folds and thrusts. These take the form of a series of ridges radiating out from the epicentre of the drip but with contraction intensifying towards the centre. As in previous experiments, we attribute the pattern to the self organization of the three dimensional flow into a network of polygonal cells (e.g., Talbot and Jackson 1987).

An arc of extension surrounds the contractional zone (Fig. 12*c*). This is delineated by a band of stretched grid that shows the beige and red colours of the lower crust and mantle lithosphere, respectively, that is exhumed. As shown in the numerical experiments, the proximal extension is driven by lateral entrainment of mantle lithosphere towards the downgoing drip. By the end of the experiment, extension is so extreme that sub-lithospheric mantle is exposed at the surface. The arcuate shape of the extension in experiment DA1 may be influenced by the cylindrical geometry of the modeling tank. In other similar experiments in a rectangular tank, we have observed angled segments of extension; some with three pronged segments akin to spreading triple junctions (Pysklywec and Cruden 2004).

A post-mortem examination of the experiment reveals a number interesting details of the mantle-crust evolution. Figures 12*d* and 12*e* show two views of the experiment after it was terminated and the top layer brittle crust (microspheres) was vacuumed off the top. The beige material is ductile lower crust, and the red material is mantle lithosphere. An oblique view of the top surface clearly shows the folded ridge pattern associated with the contraction and accumulation of lower crust directly above the drip position (Fig. 12*d*). Even with the presence of an undeforming, overlying stronger (e.g., thicker), brittle crustal layer, the lower crust may be highly deformed and mobile in response to underlying mantle flow (Pysklywec and Cruden 2004). A cut section across the drip shows significant entrainment of lower crustal material to depth within the downgoing mantle lithosphere (Fig. 12*e*). The volume of entrained material and depth are considerably greater than in either of the numerical experiments (Figs. 9, 10). This is likely owing to the lower viscosity contrast between mantle lithosphere and crust in DA1 compared with D1 and D2. Essentially, in the analogue experiment there is greater coupling between crust and mantle lithosphere.

Numerical models of delaminating lithospheric removal

Experiment DL1 modifies the configuration to promote delamination of the mantle lithosphere (i.e., the peeling away of a coherent slice of the entire mantle lithosphere). The primary difference between the models is that a weak zone is emplaced along a portion of the crust–mantle inter-

face and cutting through the mantle lithosphere (Fig. 13, top inset). Such a zone is an important factor for allowing rapid detachment between the lithospheric layers (Morency and Doin 2004). In addition, the mantle lithosphere now yields at 120 MPa (c_0 in eq. [5], rather than having a purely viscous response. The velocity boundary conditions and initial thermal structure of the models is the same as for the dripping models (Fig. 7).

Over the first 0.6 million years of the experiment, a block of mantle lithosphere starts to sink into the mantle lithosphere as the weak zone permits sub-lithospheric mantle to begin to invade into the lithosphere (Fig. 13*a*). By 1.3 million years, a fragment of mantle lithosphere has peeled away from the crust, opening up a broad lithospheric gap (Fig. 13*b*). The Lagrangian mesh shows in contrast to D1 and D2 the descending mantle lithosphere remains relatively intact as a plate, with only some bending deformation at the delaminating hinge. The delaminated lithosphere eventually detaches, further enhancing the upper mantle flow (Fig. 13*c*). In these post-removal stages, the crust is directly exposed to hot sub-lithospheric mantle along a broad swath (Figs. 13*c*, 13*d*).

Initially, the surface topography is dominated by subsidence as the delaminating lithosphere loads the crust at the hinge point (Fig. 14*a*). Aside from undulations in the surface and Moho, the crust is largely undeformed at this stage. By 6.9 million years, the surface is elevated above the broad mantle lithosphere gap (Fig. 14*b*) as an isostatic response of the surface to replacement of cold dense mantle lithosphere by less dense mantle. The uplift feature developed first at the right side (x = 1500 km) and migrated to the left as the lithosphere peeled that way. The crust has thickened by 10 km on the left side of the gap and thinned by 8 km on the right. This is a result of traction at the base of the crust from lateral sub-lithospheric mantle flow across the mantle lithosphere gap (i.e., causing contraction and thickening towards the delaminating limb and extension and thinning in the distal zone). Clearly, the development of surface topography and crustal deformation are decidedly asymmetric with the delamination experiment, in contrast to the symmetric nature of the viscous unstable lithosphere (D1 and D2).

The peak crustal temperature in the delamination experiment DL1 is also distinct from the D1 and D2 drip models (Fig. 11). There is a rapid initial increase as the mantle lithosphere slice is removed in the first 2–3 million years. Subsequently, there is more gradual heating as sub-lithospheric mantle material circulates into the gap and heat conducts into the crust. Although less rapid than D2, the delamination provides more prolonged exposure of crust to the hot mantle as the asymmetric peeling induces continued sub-lithospheric circulation.

Such mantle lithosphere removal events — both drip and delamination — provide a mechanism for explaining anomalous crustal tectonics and volcanism in intraplate or plate boundary environments. As cited previously, this may include inferred lithospheric removal events of the southern Sierra Nevada, Andes, Himalayas, Rif-Betics, and Eastern Anatolia. Most of these examples occur within convergent plate regimes; in some cases the mantle lithosphere removal and associated deformational and thermal effects occur outside of the main orogenic zone (e.g., Himalayas, eastern Anatolia) or such effects may be superimposed on the convergent tectonics (e.g., Rif-Betics, Andes). For early Earth, Zegers and van Keken (2001) propose a drip-type instability of the eclogitic components of the lithosphere to account for uplift, extension, and heating of intracratonic regions in the middle Archean (although in contrast with Bird (1979) and this study, they term this behaviour "delamination"). Vis-

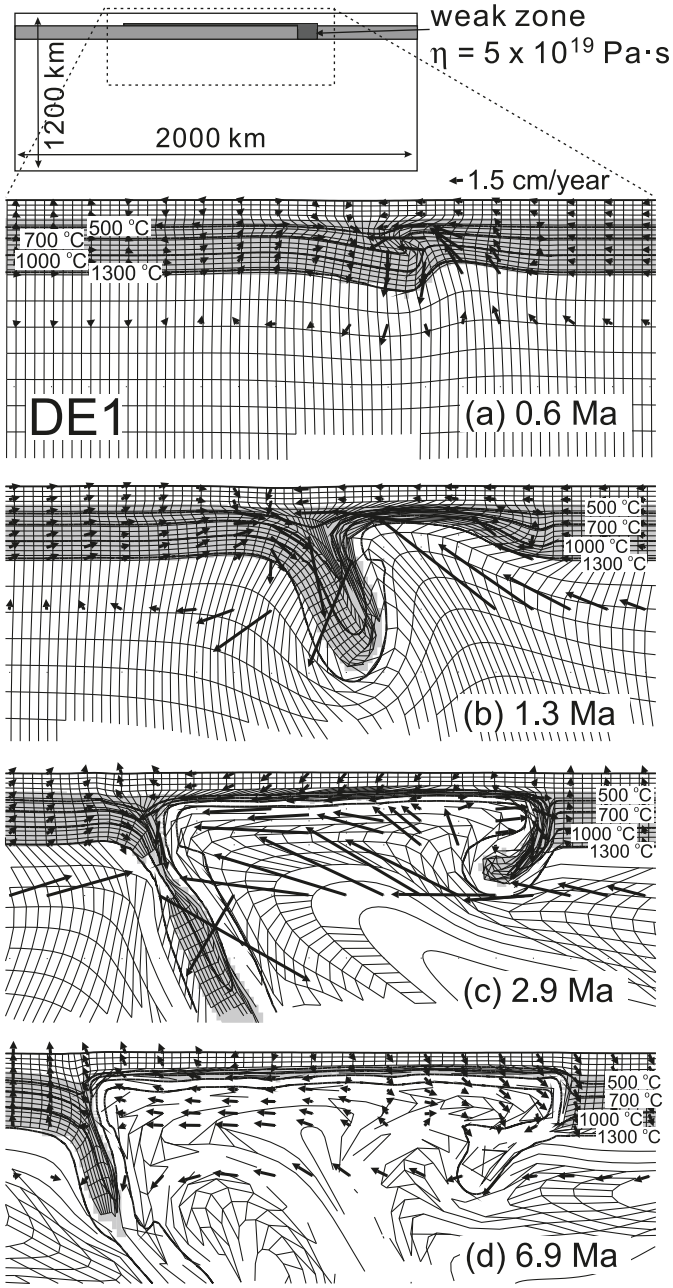

Fig. 13. Evolution of experiment DL1 at indicated times. This model is identical to the set-up shown in Fig. 7, except for some changes in configuration shown in the top inset and rheology described in the text. Mantle lithosphere domain is shaded grey. The Lagrangian mesh (initially composed of rectangular cells) at one sixth (in x-direction) and one tenth (in z-direction) the actual resolution. Instantaneous velocity vectors and selected temperature contours are superimposed. Only a portion of the full numerical solution space is shown.

cous sub-crustal dynamics have been also invoked to explain inferred tectonic deformation and volcanism at the surface of Venus as a "single-plate" planet (Bindschadler and Parmentier 1990; Lenardic et al. 1993; Lenardic and Kaula 1995; Smrekar and Parmentier 1996).

While most previous studies consider mantle lithosphere removal as a viscous dripping-type instability, our results demonstrate that delamination of mantle lithosphere may produce similar thermal and deformational responses of the crust. Namely, these include surface subsidence during active removal; surface uplift post-removal; crustal thickening–contraction directly above the foundering mantle lithosphere and possible thinning–extension adjacent to this; and heating of the crust following removal. However, several notable differences in the crustal responses exist:

(1) the topographic and thermal anomalies with delamination tend to be asymmetric, while features are largely symmetric about viscous dripping lithosphere;
(2) the surface crustal response due to delamination migrates laterally with the inherent changing position of peeling lithosphere, whereas by default with dripping lithosphere, such features are more stationary, except in cases where some external factor causes migration of the drip; and
(3) delamination is more efficient for heating the crust by producing prolonged exposure of a broad zone of the Moho to hot sub-lithospheric material.

Further studies show that the pressure–temperature (*P–T*) histories of crustal rocks may be diagnostic of dripping or delaminating mantle lithosphere (Göğüs and Pysklywec 2008*a*). Both show clockwise *P–T* paths dominated by heating; but with delamination, the metamorphism is transient and the peak heating – compression migrates, while these are relatively stationary features for viscous dripping mantle lithosphere.

Overturning mantle lithosphere

The processes of mantle lithosphere removal considered in the preceding section require that the mantle lithosphere is more dense than the underlying mantle. Recent studies of mantle xenoliths and xenocrysts have placed constraints on the secular variation in the density of sub-crustal lithosphere through Earth history (Poudjom Djomani et al. 2001; O'Reilly et al. 2001). Such analyses are interpreted to imply that there has been a progressive geochemical evolution from depleted mantle lithosphere in the Archean to a more fertile state in the Phanerozoic. Based on these measurements and assumed paleogeotherms, the cratonic mantle lithosphere in Archean and Proterozoic times may have been less dense than the underlying mantle. It is only since the Phanerozoic that the mantle lithosphere has become denser than the sub-lithospheric mantle, owing to the compositional change and cooler geotherm.

Such an alternative Precambrian lithosphere–mantle density stratification might have led to a different type of mantle lithosphere instability. Specifically, we have proposed that, in such an environment, it may be possible for mantle lithosphere to undergo an inversion or overturn (Percival and Pysklywec 2007). This model is relevant to the late-stage evolution of Archean cratons where, following a cycle

Fig. 14. Surface topography (right axis) and crust silhouette (left axis) for experiment DL1 at selected times. The surface topography is essentially a zoomed plot of the top surface of the silhouette.

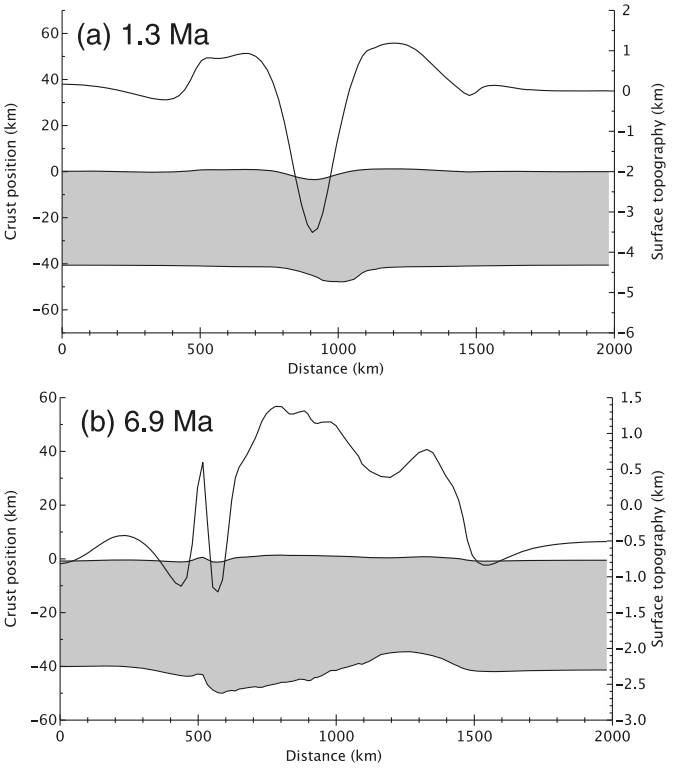

of ocean plate convergence and subduction, magmatic arc development, and arc–continent or continent–continent collision, lower crustal eclogitization creates an internal density instability within the lithosphere. Subsequently, the top-heavy mantle lithosphere and eclogite may experience an overturn with mantle lithosphere remaining in place owing to its positive buoyancy compared with the sub-lithospheric mantle.

We demonstrate how such a process might occur and the thermal and deformational manifestation of inverting mantle lithosphere. Figure 15 shows the set-up of inversion model I1. Only the lithosphere, comprising a 60 km thick crust and 140 km thick mantle lithosphere, is included in the computational domain. A block of material governed by a diabase flow law ($A = 5.05 \times 10^{-28}$ Pa$^{-4.7}$/s, $n = 4.7$, $Q = 485$ kJ/mol) is emplaced within the lower crust as a model for an eclogite layer. A dry olivine rheology (Hirth and Kohlstedt 1996) is used for the mantle lithosphere, and a modified (reduced by a factor of 4, as discussed earlier in the text) quartzite rheology (Gleason and Tullis 1995) is used for the crust. Its reference density is $\rho_{eclo} = 3500$ kg/m^3, corresponding to a typical eclogite density. In this experiment, a sub-lithospheric velocity boundary condition is applied from the left side of the box to the edge of the instability (Fig. 15) to approximate the traction associated with a shallow-dipping ($\rho_{ML} < \rho_{mantle}$), underlying subduction or mantle flow. In a wider range of models the influence of varying width and velocity magnitude of this boundary condition is considered (Percival 2007). These indicate that the results are much less sensitive to the boundary condition than they are to the width and density of the eclogite block

(see later in the text). parameters for the model are as described for the C-set of experiments. The initial geotherm represents an elevated thermal gradient through the crust (Fig. 15) that may be characteristic of Archean times (Poudjom Djomani et al. 2001). Throughout the experiments, the top and bottom boundaries of the box are held at 20 and 1350 °C, respectively.

In the first 7 million years, the dense eclogite block begins to descend, inducing a nearby upwards return flow (Fig. 16*a*). This rotational flow effectively results in inversion of the mantle lithosphere with lower mantle lithosphere being drawn up to the base of the crust and descent of upper mantle lithosphere and lower crust. In this experiment, no material is permitted to leave the computational box so the eclogite material pools at the bottom boundary (Fig. 16*b*). In other experiments, the eclogite was removed from the solution space upon reaching the lower boundary Percival 2007, but the differences in behaviour of the models with this modification are minor.

The inversion process is rapid, resulting in effective advection of the high basal-lithosphere temperatures upwards into the crust (Fig. 17*a*). The hot pulse for I1 rises to 1070 °C and gradually decreases as the lithosphere cools to equilibrate thermally (Fig. 16*c*). Figure 17*b* shows the temperatures along the full width of the solution space at a depth horizon of 58 km (i.e., near the base of the crust). This indicates that the thermal disturbance associated with mantle lithosphere inversion is uneven within the crust. Initially (7 million years), there is a decrease in crustal temperatures as the eclogite block descends and depresses the lower crustal isotherms (Fig. 17*b*). By 13 million years, there is a region of highly elevated temperatures $\sim$300 km wide, but immediately adjacent to this, temperatures are still low. The width of the elevated temperatures is governed by the width of the emplaced eclogite block Percival 2007. By later stages (39 million years), the temperature is characterized by a broad, but diminishing, high above the inversion zone.

Variations in the viscous rheology of the mantle lithosphere result in a temporal delay or advance of the heating pulse but not in the qualitative behaviour of the model (Fig. 17*a*). For example, with a wet olivine flow rheology (Hirth and Kohlstedt 1996) the heating occurs $\sim$5 million years earlier, whereas with an olivine flow law based on (Chopra and Paterson 1984), the stronger mantle lithosphere still overturns, although the process is delayed by $\sim$3 million years. Investigations of a wider range of material rheologies in the model are described in Percival (2007).

We also consider the thermal consequences of a model in which we promote a viscous dripping descent of the dense eclogite block through the mantle lithosphere (DRE, Fig. 17*a*). It has been suggested that the eclogite may pass through the lithosphere as a Rayleigh-Taylor type viscous flow (Zegers and van Keken 2001); we consider the thermal consequences of such a process. For this set of experiments, we reduced the viscosity of the eclogite layer by a factor of 50 and mantle lithosphere by a factor of 5, and removed the influence of any sub-lithospheric tractions. No geometric perturbation is required (e.g., D1, D2); rather the finite-width, dense eclogite is sufficient to initiate instability. In this experiment, there is rapid descent of the eclogite, but

Fig. 15. Illustration of the setup of the inversion "I1" experiment. Rheologies for shaded material domains are explained in the text. The eclogite block is 150 km wide and 20 km thick. A horizontal velocity (at a somewhat arbitrary rate of 5 cm/year) is imposed along a portion (as denoted) of the base of the lithosphere to approximate sub-lithospheric tractions on an orogenic root from convective mantle flow or underlying subduction.

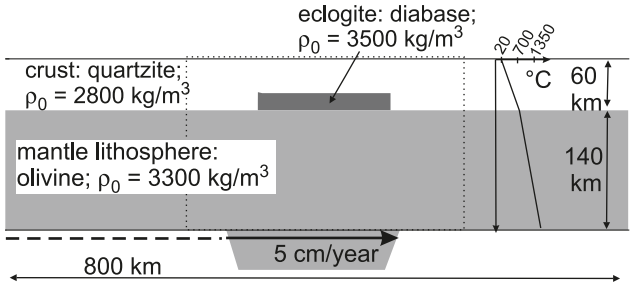

the upward return flow of mantle lithosphere is rather diffuse and broadly distributed. Consequently, the thermal signature at the base of the crust is very muted, rising only several tens of degrees above the nominal level (Fig. 17*a*). This is not to say that eclogite does not drip through the lithosphere, only that advection of mantle temperatures to the base of the crust is considerably more efficient if a bulk section of the mantle lithosphere overturns.

The thermal signature of the inversion models is comparable to that associated with the rapidly dripping mantle lithosphere model D2 (and less so, the delamination model DL1). However, the process is very different in that it allows mantle lithosphere to remain in situ during the crustal heating. This is important because it resolves a fundamental paradox relating to the evolution of Archean cratons. Namely, late-Archean granitic magmatism (so-called "granite blooms") is widespread across the Superior and Slave cratons (Cruden 2006). Such events would require significant input of heat into the crust, such as from the mantle thermal reservoir. However, xenolith studies suggest that the crust and mantle lithosphere of these cratons are of similar age (Griffin et al. 1999; Grütter et al. 1999; Aulbach et al. 2004), implying a long-term conjoined crust and mantle lithosphere. This would preclude crustal heating mechanisms through mantle lithosphere removal as described in the preceding section (experiments D1, D2, DL1). An overturning mantle lithosphere reconciles the paradox by efficiently heating the crust, while remaining rooted to the crust. We envision a closely timed series of these inversion events to account for the broad extent of crustal heating across the Superior and Slave cratons. Indeed, inversion instability in one region can trigger similar events in adjacent lithosphere.

An overturned mantle lithosphere is consistent with a host of other observations on the geology of Archean cratons. The results build on previous ideas for Archean vertical tectonics in the crust (West and Mareschal 1979; Mareschal and West 1980) by considering the coupling of mantle lithosphere dynamics to the crust. As described earlier in the text, a thermal spike accompanies lithosphere overturn and decays over a ca. 40 million year period. This time window corresponds to the post-tectonic emplacement of abundant crust-derived granitic plutons and associated low-pressure, high-temperature metamorphism experienced by most

Fig. 16. Evolution of experiment I1 at indicated times. Mantle lithosphere domain is shaded light grey and eclogite block is dark grey. The Lagrangian mesh (initially composed of rectangular cells) at one sixth (in *x*-direction) and one tenth (in *z*-direction) the actual resolution. Instantaneous velocity vectors and selected temperature contours are superimposed. Only a portion of the full numerical solution space is shown (see Fig. 15).

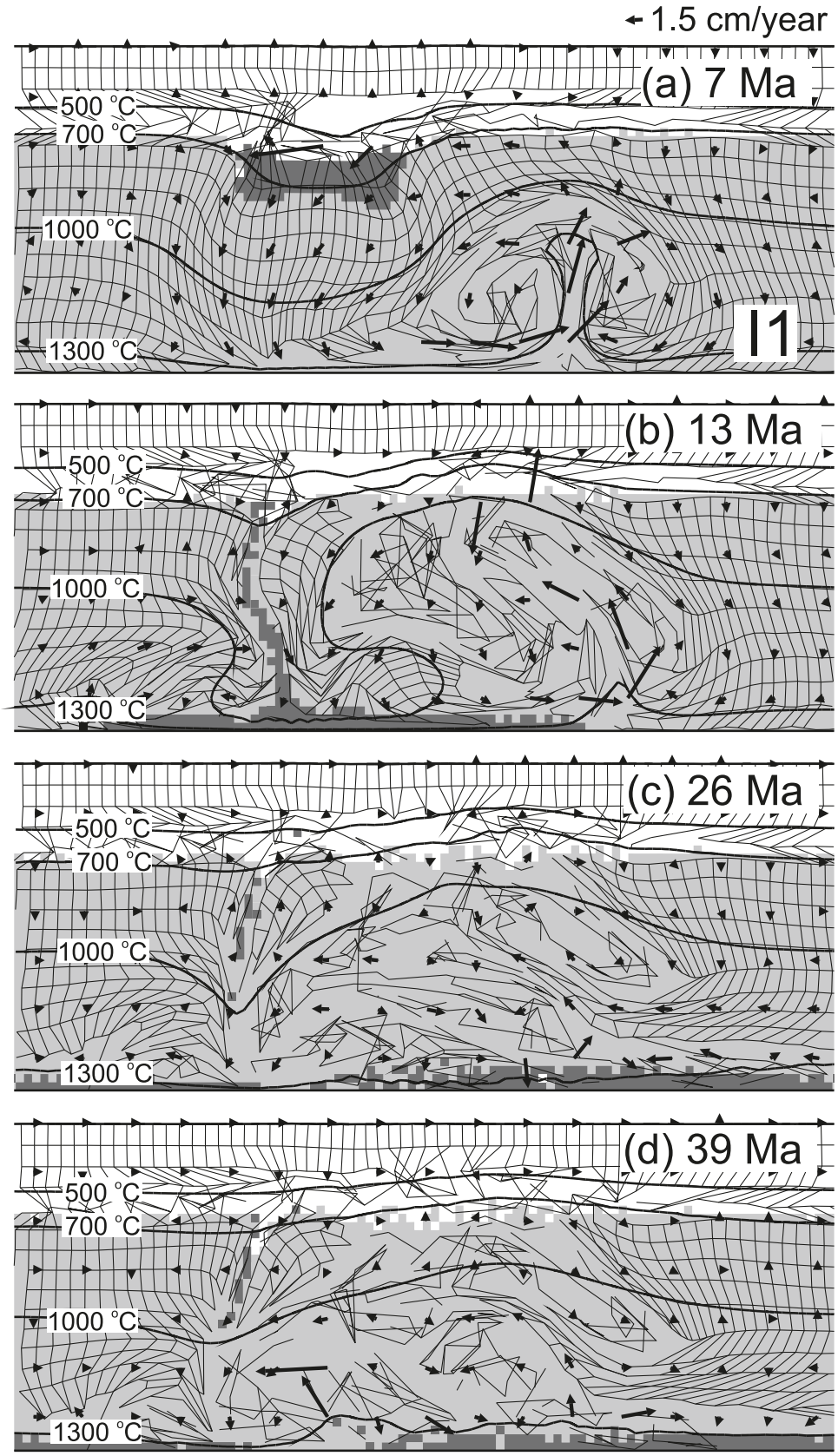

Fig. 17. (*a*) Plot of peak crustal temperature versus time for various experiments: I1, experiment shown; CP, same as I1, but a (chopra 1984) dry olivine rheology is used for mantle lithosphere; HKW, same as I1, but a hirth1996 wet olivine rheology is used for mantle lithosphere; DRE, dripping eclogite model as explained in the text. (*b*) Plot of crustal temperature at a depth horizon of 58 km for experiment I1 at three different time intervals.

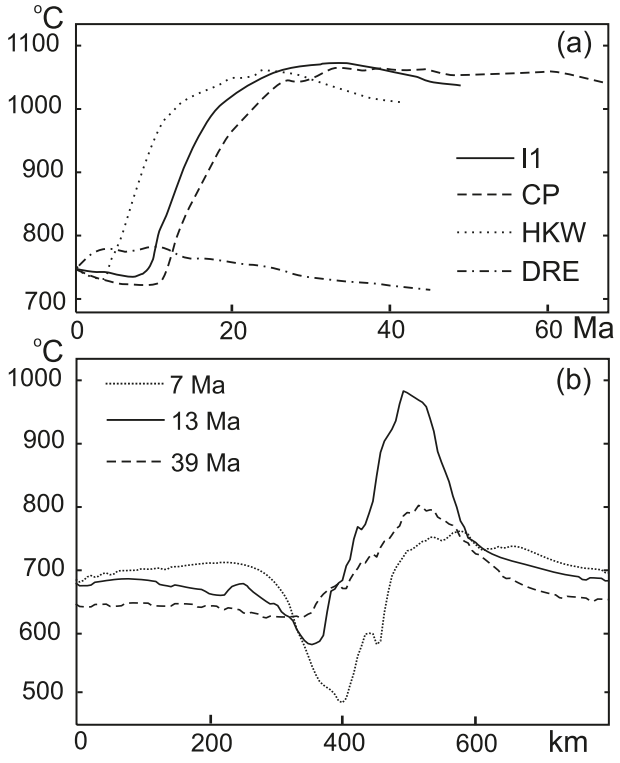

Archean cratons (Percival et al. 2006, Percival and Pysklywec 2007). As erosion levels are generally modest in Archean terranes, alternative models of crustal over-thickening and thermal relaxation to explain that these features are not applicable. Another consequence of the overturn process is production of a transient topographic depression. This phenomenon could explain the deposition of "Timiskaming-type" conglomerates in most Archean cratons: late-tectonic, coarse clastic rocks that are themselves metamorphosed. Removal of a section of dense mafic lower crust through the overturn process could explain the generally intermediate granulite composition of the present basal crust of Archean terranes (Durrheim and Mooney 1994; Musacchio et al. 2004), where mafic residues of crust-generating processes could be expected (Whalen et al. 2002).

Samples of lithospheric mantle transported to the surface in kimberlite pipes are similarly consistent with lithospheric overturn. Many garnet-bearing xenoliths exhibit geochemical evidence of melt extraction in the spinel stability field (Canil 2004), implying a history of depletion at shallow lithosphere levels and subsequent recrystallization at higher pressures. The pressure change could have been a consequence of the overturn process. Interestingly, diamond growth could have been enhanced in the central part of the overturning cell owing to reactions in the vicinity of the graphite-diamond boundary (Percival 2007).

Discussion

Geodynamic experiments demonstrate possible modes of deformation of the continental mantle lithosphere and the relationship to the tectonic evolution of the crust:

(1) During the initial stages of continental plate collision, the mantle lithosphere is characterized by plate-like behavior associated with underthrusting–subduction of the upper regions and distributed thickening and Rayleigh-Taylor viscous instability of the lower portion. Depending on the material rheology, temperature regime, and imposed convergence velocity, the deforming mantle lithosphere demonstrates various combinations of the suduction or dripping behavioural modes. Further, the imposition of surface erosion can change the dynamics of the deep lithosphere by altering the evolution of the coupled crustal layer. As continental collision develops, it tends to modify behaviour (e.g., with plate steepening, ablative or reversed plate consumption, or slab break-off). Compared with dense ocean lithosphere, which usually undergoes long-term stable subduction at convergence, we find that the juxtaposition of buoyant ("unsubductable") crust and dense mantle lithosphere in continental lithosphere gives rise to more variable plate behaviour.

(2) Dense mantle lithosphere may be actively removed from the lithosphere by processes of viscous instability–dripping or delamination. The processes are different, as the former describes distinctly "unplate-like" viscous behaviour of the mantle lithosphere, whereas the latter involves the descent of a coherent sliver of the mantle lithosphere layer. Accordingly, the crustal response to either of these removal events differs. Dripping mantle lithosphere results in a symmetric pattern of surface uplift and crustal heating centred above the removal, where the degree of heating is governed by the amount of mantle lithosphere that is removed. Delamination of mantle lithosphere induces asymmetric patterns of topography and heating that migrate with the peeling lithosphere. The crustal heating event associated with delamination will be pronounced because it inherently involves removal of the entire mantle lithosphere and direct exposure of the crust to hot mantle. Crustal deformation (zones of bulk or localized contraction and extension) driven by the removal processes can be appreciable and may account for tectonic activity within certain intraplate regions on Earth or on single-plate planets such as Venus.

(3) The emplacement of post-orogenic eclogite in the lower crust and basal traction may trigger rapid overturn or inversion of the mantle lithosphere. This advects highly elevated temperatures (by $\sim$300 °C) to the base of the crust across a width corresponding to the lateral extent of the eclogite. Such overturn is robust among a range of material rheologies and acts as a much more efficient crustal heating mechanism than dripping-type viscous instability of the eclogite. The process may account for the inferred heating associated with the presence of widespread granite blooms across many Archean cratons. Specifically, an overturn stabilization of the lithosphere reconciles the need for bringing mantle-level temperatures to the crust while retaining mantle lithosphere in situ adjacent to the crust.

There is a relationship between mantle lithosphere convergence and removal of the mantle where they may occur concurrently or in transition from one to another. For example, convergent mantle lithosphere undergoing accretion and thickening can evolve to a mantle lithosphere thinning mode if the convergence rate is sufficiently low relative to the rate of descent of the unstable mantle lithosphere (Pysklywec et al. 2000). Alternatively, the process of gravitational instability of the mantle lithosphere requires a perturbation to the base of the lithosphere to initiate flow (with an initial growth rate higher than the rate of thermal diffusion, which may negate the mantle lithosphere perturbation). Plate shortening and thickening of the mantle lithosphere can furnish this initial perturbation to start viscous instability of the lower lithosphere (Conrad and Molnar 1997, Molnar et al. 1998).

It may be useful to clarify the relation of our work in the context of the issue of long-term stability of cratonic mantle lithosphere. There is a substantial body of geophysical, geochemical, and geological evidence that suggests cratonic mantle lithosphere (as "roots" or "keels") has been largely stable over long time scales (e.g., Jordan 1978; Rudnick 1998; Lenardic and Moresi 1999; Shapiro et al. 1999; Lee et al. 2001; Shirey et al. 2002; Kelly et al. 2003). We propose that in certain cases during the Archean, in situ overturn of the mantle lithosphere may have made up a stage in the stabilization process. Although cratonic roots may have remained tectonically inactive, selected regions of the continental plates — both in the interior and at the margins — are not stabilized by composition or density. It is such regions, as at collision and with particular density instablities, that we demonstrate that continental mantle lithosphere can be dynamically active and a driving force for crustal tectonics.

In the collisional experiments, there is no pre-existing oceanic subduction; instead, an emplaced weak "seed" in the model approximates pre-existing geological heterogeneities that initially locate the region for plate collision in the otherwise homogeneous model lithosphere. Oceanic subduction can often precede collision and such an event may have thermal consequences for the over-riding lithosphere (Hyndman and Lewis 1999; Currie and Hyndman 2006). In these cases, one might expect a hotter and weaker lithosphere — possibly localized laterally to the collisional boundary — which could modify the style of continental collision. Some justification for this assumption may be provided by the propensity for oceanic lithosphere to detach from the surface at a continental collision (Davies and von Blanckenburg 1995). Furthermore, certain regions of continental plate convergence — such as the prototype for this studty, South Island, New Zealand — were not immediately preceded by the subduction of intervening oceanic lithosphere. However, it should be recognized that evolution of collision in a continental back-arc could modify the results.

The experiments are restricted to the upper mantle-scale domain ($<\sim$600–700 km depth). The motivation for this is largely a practical consideration of the computational modeling: to enable high-resolution calculations within the deforming lithosphere, it becomes expedient to restrict the lower extent of the box. We chose the bottom of the solution space to correspond to the upper mantle – lower mantle boundary for several reasons. Firstly, estimates of mean mantle viscosity suggest there is an increase in viscosity of up to two orders of magnitude from the upper to lower mantle through this region (Mitrovica and Forte 1997) that would inhibit flow through this level. Furthermore, the endothermic phase transformation of olivine at $\sim$670 km depth may introduce buoyancy effects that may significantly hinder mass flux across the upper mantle – lower mantle boundary (Christensen and Yuen 1984, 1985). If one considers the behaviour of material at this interface in the Earth inferred from seismic techniques, there is evidence for both penetration and stagnation of downgoing material. Certain subducting plates, such as the Farallon slab beneath North and Central America, seem to descend deeply into the lower mantle, reaching the core–mantle boundary Grand 1994. On the other hand, a broad suite of tomographic images indicate that a significant number of slabs may deflect and accumulate in the transition zone (Fukao et al. 1992; van der Hilst 1995; Fukao et al. 2001). The inherent assumption in the models is that the upper mantle – lower mantle boundary is an impediment to flow like these latter examples.

Acknowledgements

This work was funded by NSERC Discovery and Lithoprobe Supporting Geoscience grants. Numerical calculations used software developed by Philippe Fullsack and augmented by the authors. We acknowledge Malcolm Shaw for contributions with the laboratory experiments. We thank Claire Currie, an anonymous referee, and Ron Clowes as Associate Editor for constructive reviews of the original manuscript.

References

Aulbach, S., Griffin, W.L., Pearson, N.J., O'Reilly, S.Y., Kivi, K., and Doyle, B.J. 2004. Mantle formation and evolution, Slave craton: constraints from HSE abundances and Re–Os isotope systematics of sulfide inclusions in mantle xenocrysts. Chemical Geology, **208**(1-4): 61–88. doi:10.1016/j.chemgeo.2004.04.006.

Batt, G.E., and Braun, J. 1997. On the thermomechanical evolution of compressional orogens. Geophysical Journal International, **128**(2): 364–382. doi:10.1111/j.1365-246X.1997.tb01561.x.

Beaumont, C., Fullsack, P., and Hamilton, J. 1992. Erosional control of active compressional orogens. *In* Thrust tectonics. *Edited by* K.R. McClay. Chapman and Hall, New York, N.Y., pp. 1–18.

Beaumont, C., Kamp, P.J.J., Hamilton, J., and Fullsack, P. 1996. The continental collision zone, South Island, New Zealand: Comparison of geodynamical models and observations. Journal of Geophysical Research, **101**(B2): 3333–3359. doi:10.1029/95JB02401.

Betts, P.G. 1999. Palaeoproterozoic mid-basin inversion in the northern Mt. Isa terrane, Queensland. Australian Journal of Earth Sciences, **46**(5): 735–748. doi:10.1046/j.1440-0952.1999.00741.x.

Bindschadler, D.L., and Parmentier, E.M. 1990. Mantle flow tectonics: The influence of a ductile lower crust and implications for the formation of topographic uplands on Venus. Journal of Geophysical Research, **95**(B13): 21 329 – 21 344. doi:10.1029/JB095iB13p21329.

Bird, P. 1979. Continental delamination and the Colorado Plateau. Journal of Geophysical Research, **84**: 7561–7571.

Bostock, M.G. 1997. Anisotropic upper-mantle stratigraphy and architecture of the Slave craton. Nature, **390**(6658): 392–395. doi:10.1038/37102.

Bostock, M.G. 1998. Mantle stratigraphy and the evolution of the Slave province. Journal of Geophysical Research, **103**(B9): 21 183 – 21 200. doi:10.1029/98JB01069.

Buck, W.R., and Toksöz, M.N. 1983. Thermal effects of continental collisions: Thickening a variable viscosity lithosphere. Tectonophysics, **100**(1–3): 53–69. doi:10.1016/0040-1951(83)90178-6.

Buiter, S.J.H., Govers, R., and Wortel, M. 2001. A modelling study of vertical surface displacements at convergent plate margins. Geophysical Journal International, **147**(2): 415–427. doi:10.1046/j.1365-246X.2001.00545.x.

Calvert, A.J., Sawyer, E.W., Davis, W.J., and Ludden, J. 1995. Archaean subduction inferred from seismic images of a mantle suture in the Superior province. Nature, **375**(6533): 670–674. doi:10.1038/375670a0.

Canil, D. 2004. Mildly incompatible elements in peridotites and the origin of mantle lithosphere. Lithos, **77**(1–4): 375–393. doi:10.1016/j.lithos.2004.04.014.

Carbno, G.B., and Canil, D. 2002. Mantle stratigraphy beneath the southwest Slave Province, Canada: constraints from garnet geochemistry in the Drybones Bay kimberlite. Journal of Petrology, **43**: 129–142. doi:10.1093/petrology/43.1.129.

Chen, W.-P., and Tseng, T.-L. 2007. Small 660-km seismic discontinuity beneath Tibet implies resting ground for detached lithosphere. Journal of Geophysical Research, **112**(B5): B05309. doi:10.1029/2006JB004607.

Chopra, P.N., and Paterson, M.S. 1984. The role of water in the deformation of dunite. Journal of Geophysical Research, **89**(B9): 7861–7876. doi:10.1029/JB089iB09p07861.

Christensen, U.R., and Yuen, D.A. 1984. The interaction of a subducting slab with a chemical or phase boundary. Journal of Geophysical Research, **89**(B6): 4389–4402. doi:10.1029/JB089iB06p04389.

Christensen, U.R., and Yuen, D.A. 1985. Layered convection induced by phase changes. Journal of Geophysical Research, **90**(B12): 10 291 – 10 300. doi:10.1029/JB090iB12p10291.

Conrad, C.P., and Molnar, P. 1997. The growth of Rayleigh-Taylor-type instabilities in the lithosphere for various rheological and density structures. Geophysical Journal International, **129**(1): 95–112. doi:10.1111/j.1365-246X.1997.tb00939.x.

Cruden, A.R. 2006. Emplacement and growth of plutons: implications for rates of melting and mass transfer in continental crust. *In* Evolution and differentiation of the continental crust. *Edited by* M. Brown and T. Rushmer. Cambridge University Press, Cambridge, UK., pp. 455–519.

Currie, C.A., and Hyndman, R.D. 2006. The thermal structure of subduction zone back arcs. Journal of Geophysical Research, **111**(B8): B08404. doi:10.1029/2005JB004024.

Davies, J.H., and von Blanckenburg, F. 1995. Slab breakoff: A model of lithosphere detachment and its test in the magmatism and deformation of collisional orogens. Earth and Planetary Science Letters, **129**(1–4): 85–102. doi:10.1016/0012-821X(94)00237-S.

Davy, P., and Cobbold, P.R. 1988. Indentation tectonics in nature and experiment. 1. Experiments scaled for gravity. Bulletin of the Geological Institutions of the University of Uppsala, **14**: 129–141.

Davy, P., and Cobbold, P.R. 1991. Experiments on shortening of a 4-layer model of the continental lithosphere. Tectonophysics, **188**(1–2): 1–25. doi:10.1016/0040-1951(91)90311-F.

Durrheim, R.J., and Mooney, W.D. 1994. Evolution of the Precambrian lithosphere — Seismological and geochemical constraints. Journal of Geophysical Research, **99**(B8): 15 359 – 15 374. doi:10.1029/94JB00138.

Ellis, S., Beavan, J., and Eberhart-Phillips, D. 2006. Bounds on the width of mantle lithosphere flow derived from surface geodetic measurements: application to the central Southern Alps, New Zealand. Geophysical Journal International, **166**(1): 403–417. doi:10.1111/j.1365-246X.2006.02918.x.

England, P., and Houseman, G.A. 1989. Extension during continental convergence, with application to the Tibetan Plateau. Journal of Geophysical Research, **94**(B12): 17 561 – 17 579. doi:10.1029/JB094iB12p17561.

Fleitout, L., and Froidevaux, C. 1982. Tectonics and topography for a lithosphere containing density heterogeneities. Tectonics, **1**(1): 21–56. doi:10.1029/TC001i001p00021.

Fukao, Y., Obayashi, M., Inoue, H., and Nenbai, M. 1992. Subducting slabs stagnant in the mantle transition zone. Journal of Geophysical Research, **97**(B4): 4809–4822. doi:10.1029/91JB02749.

Fukao, Y., Widiyantoro, S., and Obayashi, M. 2001. Stagnant slabs in the upper and lower mantle transiton region. Reviews of Geophysics, **39**(3): 291–323. doi:10.1029/1999RG000068.

Fullsack, P. 1995. An arbitrary Lagrangian–Eulerian formulation for creeping flows and applications in tectonic models. Geophysical Journal International, **120**(1): 1–23. doi:10.1111/j.1365-246X.1995.tb05908.x.

Gleason, G.C., and Tullis, J. 1995. A flow law for dislocation creep of quartz aggregates determined with the molten salt cell. Tectonophysics, **247**(1–4): 1–23. doi:10.1016/0040-1951(95)00011-B.

Göğüs, O., and Pysklywec, R.N. 2008*a*. Mantle lithosphere delamination driving plateau uplift and syn-convergent extension in Eastern Anatolia. Geology, **36**(9): 723–726. doi:10.1130/G24982A.1.

Göğüs, O., and Pysklywec, R.N. 2008*b*. Near surface diagnostics of dripping or delaminating lithosphere. Journal of Geophysical Research, 113, 11 p.

Grand, S. 1994. Mantle hear structure beneath the Americas and surrounding oceans. Journal of Geophysical Research, **99**(B6): 11 591 – 11 621. doi:10.1029/94JB00042.

Griffin, W.L., Doyle, B.J., Ryan, C., Pearson, N.J., O'Reilly, S.Y., Davies, R.M., et al. 1999. Layered mantle lithosphere in the Lac de Gras area, Slave Craton: composition, structure and origin. Journal of Petrology, **40**(5): 705–727. doi:10.1093/petrology/40.5.705.

Grütter, H.S., Apter, D.B., and Kong, J. 1999. Crust-mantle coupling; evidence from mantle-derived xenocrystic garnets. *In* Proceedings of the 7th International Kimberlite Conference. *Edited by* J.J. Gurney, J.L. Gurney, M.D. Pascoe, and S.H. Richardson. The J.B. Dawson Vol., pp. 307–313.

Hirth, G., and Kohlstedt, D.L. 1996. Water in the oceanic upper mantle: Implications for rheology, melt extraction and the evolution of the lithosphere. Earth and Planetary Science Letters, **144**(1–2): 93–108. doi:10.1016/0012-821X(96)00154-9.

Houseman, G.A., and Molnar, P. 1997. Gravitational (Rayleigh-Taylor) instability of a layer with non-linear viscosity and convective thinning of continental lithosphere. Geophysical Journal International, **128**(1): 125–150. doi:10.1111/j.1365-246X.1997.tb04075.x.

Houseman, G.A., McKenzie, D.P., and Molnar, P. 1981. Convective instability of a thickened boundary layer and its relevance for the thermal evolution of continental convergent belts. Journal of Geophysical Research, **86**(B7): 6115–6132. doi:10.1029/JB086iB07p06115.

Houseman, G.A., Neil, E.A., and Kohler, M.D. 2000. Lithospheric instability beneath the Transverse Ranges of California. Journal of Geophysical Research, **105**(B7): 16 237 – 16 250. doi:10.1029/2000JB900118.

Hyndman, R.D., and Lewis, T.J. 1999. Geophysical consequences of the Cordillera–Craton thermal transition in southwestern Canada: thermal regimes in the continental and oceanic lithosphere. Tectonophysics, **306**: 397–422. doi:10.1016/S0040-1951(99)00068-2.

Jones, A.G., Ferguson, I.J., Chave, A.D., Evans, R.L., and McNeice, G.W. 2001. Electric lithosphere of the Slave craton. Geology, **29**(5): 423–426. doi:10.1130/0091-7613(2001)029<0423:ELOTSC>2.0.CO;2.

Jordan, T.H. 1978. Composition and development of the continental tectosphere. Nature, **274**(5671): 544–548. doi:10.1038/274544a0.

Kay, W.W., and Kay, S. 1993. Delamination and delamination magmatism. Tectonophysics, **219**(1–3): 177–189. doi:10.1016/0040-1951(93)90295-U.

Kelly, R., Kelemen, P., and Jull, M. 2003. Buoyancy of the continental upper mantle. Geochemistry Geophysics Geosystems, **4**(2): 1017. doi:10.1029/2002GC000399.

Keskin, M. 2003. Magma generation by slab steepening and breakoff beneath a subduction–accretion complex: An alternative model for collision-related volcanism in Eastern Anatolia, Turkey. Geophysical Research Letters, **30**(24): 8046 doi:10.1029/2003GL018019.

Koons, P.O. 1995. Modeling the topographic evolution of collisional belts. Annual Review of Earth and Planetary Sciences, **23**(1): 375–408. doi:10.1146/annurev.ea.23.050195.002111.

Kopylova, M.G., and Russell, J.K. 2000. Chemical stratification of cratonic lithosphere: constraints from the Northern Slave craton, Canada. Earth and Planetary Science Letters, **181**: 71–87. doi:10.1016/S0012-821X(00)00187-4.

Lachenbruch, A.H., and Sass, J.H. 1977. Heat flow in the United States and the thermal regime of the crust. *In* The Earth's crust, its nature and physical properties. *Edited by* J.G. Heacock. American Geophysical Union, Geophysical Monograph 20, pp. 626–675.

Lee, C.T., Yin, Q., Rudnick, R.L., Chesley, J.T., and Jacobsen, S.B. 2000. Os isotropic evidence for mesozoic removal of lithospheric mantle beneath the Sierra Nevada, California. Science, **289**(5486): 1912–1916. doi:10.1126/science.289.5486.1912.

Lee, C.T., Yin, Q., Rudnick, R.L., and Jacobsen, S.B. 2001. Preservation of ancient and fertile lithospheric mantle beneath the southwestern United States. Nature, **411**(6833): 69–73. doi:10.1038/35075048.

Lenardic, A., and Kaula, W.M. 1995. More thoughts on convergent crustal plateau formation and mantle dynamics with regard to Tibet. Journal of Geophysical Research, **100**(B8): 15 193 – 15 203. doi:10.1029/95JB01289.

Lenardic, A., and Moresi, L.N. 1999. Some thoughts on the stability of cratonic lithosphere: Effects of buoyancy and viscosity. Journal of Geophysical Research, **104**(B6): 12 747 – 12 758. doi:10.1029/1999JB900035.

Lenardic, A., Kaula, W.M., and Bindschadler, D.L. 1993. A mechanism for crustal recycling on Venus. Journal of Geophysical Research, **98**(E10): 18697–18705. doi:10.1029/93JE01799.

Mareschal, J.C., and West, G. 1980. A model for Archaean tectonism. Part 2 — Numerical models of vertical tectonism in greenstone belts. Canadian Journal of Earth Sciences, **17**: 60–72.

Marotta, A.M., Fernandez, M., and Sabadini, R. 1999. The onset of extension during lithospheric shortening: A two-dimensional thermomechanical model for lithospheric unrooting. Geophysical Journal International, **139**(1): 98–114. doi:10.1046/j.1365-246X.1999.00922.x.

McLaren, S., and Sandiford, M. 2001. Long-term thermal consequences of tectonic activity at Mt. Isa. *In* Implications for polyphase tectonism in the Proterozoic. Geological Society, Special Publication 184, pp. 219–236.

McLaren, S., Sandiford, M., and Hand, M. 1999. High radiogenic heat-producing granites and metamorphism — an example from the western Mount Isa inlier, Australia. Geology, **27**(8): 679–682. doi:10.1130/0091-7613(1999)027<0679:HRHPGA>2.3.CO;2.

Meissner, R., and Mooney, W. 1998. Weakness of the lower continental crust: a condition for delamination, uplift, and escape. Tectonophysics, **296**(1–2): 47–60. doi:10.1016/S0040-1951(98)00136-X.

Mitrovica, J.X., and Forte, A.M. 1997. The radial profile of mantle viscosity: Results from the joint inversion of convection of post glacial rebound observables. Journal of Geophysical Research, **102**(B2): 2751–2769. doi:10.1029/96JB03175.

Molnar, P., Houseman, G.A., and Conrad, C.P. 1998. Rayleigh-Taylor-type instability and convective thinning of mechanically thickened lithosphere: Effects of non-linear viscosity decreasing exponentially with depth and of horizontal shortening of the layer. Geophysical Journal International, **133**(3): 568–584. doi:10.1046/j.1365-246X.1998.00510.x.

Molnar, P., Anderson, H.J., Audoine, E., Eberhart-Phillips, D., Gledhill, K.R., Klosko, E.R., et al. 1999. Continuous deformation versus faulting through the continental lithosphere of New Zealand. Science, **286**(5439): 516–519. doi:10.1126/science.286.5439.516.

Montgomery, D.R., and Brandon, M.T. 2002. Topographic controls on erosion rates in tectonically active mountain ranges. Earth and Planetary Science Letters, **201**(3–4): 481–489. doi:10.1016/S0012-821X(02)00725-2.

Morency, C., and Doin, M.-P. 2004. Numerical simulations of mantle lithospheric delamination. Journal of Geophysical Research, **109**(B3): B03410. doi:10.1029/2003JB002414.

Musacchio, G., White, D.J., Asudeh, I., and Thomson, C.J. 2004. Lithospheric structure and composition of the Archean western Superior Province from seismic refraction/wide-angle reflection and gravity modeling. Journal of Geophysical Research, **109**(B3): B03304. doi:10.1029/2003JB002427.

Neil, E.A., and Houseman, G.A. 1999. Rayleigh-Taylor instability of the upper mantle and its role in intraplate orogeny. Geophysical Journal International, **138**(1): 89–107. doi:10.1046/j.1365-246x.1999.00841.x.

O'Dea, M.G., Lister, G.S., MacCready, T., Betts, P.G., Oliver, N.H.S., Pound, K.S., Huang, W., and Valenta, R.K. 1997. Geodynamic evolution of the Proterozoic Mount Isa terrain. *In* Orogeny through time. *Edited by* J.P. Burg and M. Ford. Geological Society, Special Publication 121, pp. 99–122.

O'Reilly, S.Y., Griffin, W.L., Poudjom Djomani, Y.H., and Morgan, P. 2001. Are lithospheres forever? Tracking changes in subcontinental lithospheric mantle through time. GSA Today, **11**(4): 4–10. doi:10.1130/1052-5173(2001)011<0004:ALFTCI>2.0.CO;2.

Percival, J.A. 2007. Geology and metallogeny of the Superior Province. *In* Mineral deposits of Canada: a synthesis of major deposit-types, district metallogeny, the evolution of geological provinces, and exploration methods. *Edited by* W.D. Goodfellow. Geological Association of Canada, Mineral Deposits Subdivision, Vol. 5, pp. 903–928.

Percival, J.A., and Pysklywec, R.N. 2007. Are Archean lithospheric keels inverted? Earth and Planetary Science Letters, **254**(3–4): 393–403. doi:10.1016/j.epsl.2006.11.047.

Percival, J.A., Sanborn-Barrie, M., Skulski, T., Stott, G., Helmstaedt, H., Skulski, T., and White, D.J. 2006. Tectonic evolution of the Western Superior Province from NATMAP and Lithoprobe studies. Canadian Journal of Earth Sciences, **43**(7): 1085–1117. doi:10.1139/E06-062.

Platt, J.P., and Vissers, R.L.M. 1989. Extensional collapse of thickened continental lithosphere: A working hypothesis for the Al-

boran Sea and Gibraltar Arc. Geology, **17**(6): 540–543. doi:10.1130/0091-7613(1989)017<0540:ECOTCL>2.3.CO;2.

Poudjom Djomani, Y.H., O'Reilly, S.Y., Griffin, W.L., and Morgan, P. 2001. The density structure of subcontinental lithosphere through time. Earth and Planetary Science Letters, **184**(3-4): 605–621. doi:10.1016/S0012-821X(00)00362-9.

Pourhiet, L.L., Gurnis, M., and Saleeby, J. 2006. Mantle instability beneath the Sierra Nevada Mountains in California and Death Valley extension. Earth and Planetary Science Letters, **251**(1–2): 104–119. doi:10.1016/j.epsl.2006.08.028.

Pysklywec, R.N. 2001. Evolution of subducting mantle lithosphere at a continental plate boundary. Geophysical Research Letters, **28**(23): 4399–4402. doi:10.1029/2001GL013567.

Pysklywec, R.N. 2006. Surface erosion control on the evolution of the deep lithosphere. Geology, **34**(4): 225–228. doi:10.1130/G21963.1.

Pysklywec, R.N., and Beaumont, C. 2004. Intraplate tectonics: feedback between radioactive thermal weakening and crustal deformation driven by mantle lithosphere instabilities. Earth and Planetary Science Letters, **221**(1–4): 275–292. doi:10.1016/S0012-821X(04)00098-6.

Pysklywec, R.N., and Cruden, A.R. 2004. Coupled crust–mantle dynamics and intraplate tectonics: Two-dimensional numerical and three-dimensional analogue modeling. Geochemistry Geophysics Geosystems, **5**(10): 1–22. doi:10.1029/2004GC000748.

Pysklywec, R.N., and Shahnas, M.H. 2003. Time-dependent surface topography in a coupled crust–mantle convection model. Geophysical Journal International, **154**(2): 268–278. doi:10.1046/j.1365-246X.2003.01987.x.

Pysklywec, R.N., Beaumont, C., and Fullsack, P. 2000. Modeling the behavior of the continental mantle lithosphere during plate convergence. Geology, **28**(7): 655–658. doi:10.1130/0091-7613(2000)28<655:MTBOTC>2.0.CO;2.

Pysklywec, R.N., Beaumont, C., and Fullsack, P. 2002. Lithospheric deformation during the early stages of continental collision: Numerical experiments and comparison with South Island, New Zealand. Journal of Geophysical Research, **107**(B7): 2133. doi:10.1029/2001JB000252.

Rudnick, R.L. 1998. Thermal structure, thickness and composition of continental lithosphere. Chemical Geology, **145**(3–4): 395–411. doi:10.1016/S0009-2541(97)00151-4.

Saleeby, J., Ducea, M., and Clemens-Knott, D. 2003. Production and loss of high-density batholithic root, southern Sierra Nevada. Tectonics, **22**(6): 6. doi:10.1029/2002TC001374.

Sandiford, M., and Hand, M. 1998. Controls on the locus of intraplate deformation in central Australia. Earth and Planetary Science Letters, **162**(1–4): 97–110. doi:10.1016/S0012-821X(98)00159-9.

Sandiford, M., and McLaren, S. 2002. Tectonic feedback and the ordering of heat producing elements within the continental lithosphere. Earth and Planetary Science Letters, **204**(1–2): 133–150. doi:10.1016/S0012-821X(02)00958-5.

Schmidberger, S.S., and Francis, D. 1999. Nature of the mantle roots beneath the North American craton: Mantle xenolith evidence from Somerset Island kimberlites. Lithos, **48**(1–4): 195–216. doi:10.1016/S0024-4937(99)00029-8.

Scott, D.L., Rawlings, D.J., Page, R.W., Tarlowski, C.Z., Idnurm, M., Jackson, M.J., and Southgate, P.N. 2000. Basement framework and geodynamic evolution of the Palaeoproterozoic superbasins of north-central Australia: an integrated review of geochemical, geochronological and geophysical data. Australian Journal of Earth Sciences, **47**(3): 341–380. doi:10.1046/j.1440-0952.2000.00793.x.

Scully, K., Canil, D., and Schulze, D.J. 2004. The lithospheric mantle of the Archean Superior Province as imaged by garnet xenocryst geochemistry. Chemical Geology, **207**(3–4): 189–221. doi:10.1016/j.chemgeo.2004.03.001.

Seber, D., Barazangi, M., Ibenbrahim, A., and Demnati, A. 1996. Geophysical evidence for lithospheric delamination beneath the Alboran Sea and Rif-Betic mountains. Nature, **379**(6568): 785–790. doi:10.1038/379785a0.

Sengör, A.M.C., Özeren, S., Genç, T., and Zor, E. 2003. Magma generation by slab steepening and breakoff beneath a subduction-accretion complex: An alternative model for collision-related volcanism in Eastern Anatolia, Turkey. Geophysical Research Letters, **30**(24): 8045.

Shapiro, S.S., Hager, B.H., and Jordan, T.H. 1999. Stability and dynamics of the continental tectosphere. Lithos, **48**(1–4): 115–133. doi:10.1016/S0024-4937(99)00025-0.

Shaw, R.D., Etheridge, M.A., and Lambeck, K. 1991. Development of the late Proterozoic to mid-Palaeozoic intracratonic Amadeus Basin in central Australia: A key to understanding tectonic forces in plate interiors. Tectonics, **10**(4): 688–721. doi:10.1029/90TC02417.

Shirey, S.B., Harris, J.W., Richardson, S.H., Fouch, M.J., James, D.E., Cartigny, P., Deines, P., and Viljoen, F. 2002. Diamond genesis, seismic structure, and evolution of the Kaapvaal–Zimbabwe craton. Science, **297**(5587): 1683–1686. doi:10.1126/science.1072384.

Smrekar, S.E., and Parmentier, E. 1996. The interaction of mantle plumes with surface thermal and chemical boundary layers: Applications to hotspots on Venus. Journal of Geophysical Research, **101**(B3): 5397–5410. doi:10.1029/95JB02877.

Sobolev, S.V., and Babeyko, A.Y. 2005. What drives orogeny in the Andes? Geology, **33**(8): 617–620. doi:10.1130/G21557.1.

Stern, T., Molnar, P., Okaya, D., and Eberhart-Philips, D. 2000. Teleseismic *p* wave delays and modes of shortening the mantle lithosphere beneath South Island, New Zealand. Journal of Geophysical Research, **105**(B9): 21 615 – 21 631. doi:10.1029/2000JB900166.

Talbot, C.J., and Jackson, M.P.A. 1987. Salt tectonics. Scientific American, **255**: 70–79.

Tao, W.C., and O'Connell, R.J. 1992. Ablative subduction: A two-sided alternative to the conventional subduction model. Journal of Geophysical Research, **97**(B6): 8877–8904. doi:10.1029/91JB02422.

Teng, L.S., Lee, C.T., Tsai, Y.B., and Hsiao, L.-Y. 2000. Slab breakoff as a mechanism for flipping of subduction polarity in Taiwan. Geology, **28**(2): 155–158. doi:10.1130/0091-7613(2000)28<155:SBAAMF>2.0.CO;2.

van der Hilst, R. 1995. Complex morphology of subducted lithosphere in the mantle beneath the Tonga trench. Nature, **374**(6518): 154–157. doi:10.1038/374154a0.

Van der Voo, R., Spakman, W., and Bijwaard, H. 1999. Tethyan subducted slabs under India. Earth and Planetary Science Letters, **171**(1): 7–20. doi:10.1016/S0012-821X(99)00131-4.

Wernicke, B., Clayton, R., Ducea, M., Jones, C.H., Park, S., Ruppert, S., et al. 1996. Origin of high mountains in the continents: The Southern Sierra Nevada. Science, **271**(5246): 190–193. doi:10.1126/science.271.5246.190.

West, G., and Mareschal, J.C. 1979. A model for Archaean tectonism. part 1: The thermal conditions. Canadian Journal of Earth Sciences, **16**: 1942–1950.

Whalen, J.B., Percival, J.A., McNicoll, V., and Longstaffe, F.J. 2002. A mainly crustal origin for tonalitic granitoid rocks, Superior Province, Canada: Implications for late Archean tectonomagmatic processes. Journal of Petrology, **43**(8): 1551–1570. doi:10.1093/petrology/43.8.1551.

Willett, S.D. 1999. Orogeny and orography: The effects of erosion on the structure of mountain belts. Journal of Geophysical Research, **104**(B12): 28 957 – 28 981. doi:10.1029/1999JB900248.

Willett, S., Beaumont, C., and Fullsack, P. 1993. echanical model for the tectonics of doubly vergent compressional orogens. Geology, **21**(4): 371–374. doi:10.1130/0091-7613(1993)021<0371:MMFTTO>2.3.CO;2.

Zandt, G., Gilbert, H., Owens, T.J., Ducea, M., Saleeby, J., and Jones, C.H. 2004. Active foundering of a continental arc root beneath the southern Sierra Nevada in California. Nature, **431**(7004): 41–46. doi:10.1038/nature02847.

Zegers, T.E., and van Keken, P.E. 2001. Middle Archean continent formation by crustal delamination. Geology, **29**(12): 1083–1086. doi:10.1130/0091-7613(2001)029<1083:MACFBC>2.0.CO;2.